AD-A095 255 SYSTEMS SCIENCE AND SOFTWARE LA JOLLA CA F/G 18/3
HE SIMULATION OF GROUND SHOCK-INDUCED MX TRENCH COLLAPSE.(U)
OCT 80 J C BAKER, H R KRATZ, K D PYATT DNA001-78-C-0211
UNCLASSIFIED SSS-R-79-4016 DNA-5182F NL

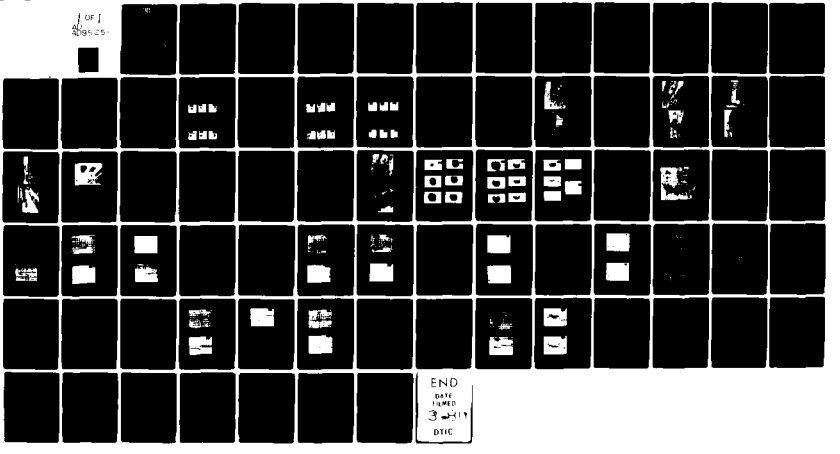

LEVEL II

12

DNA 5182F

HE SIMULATION OF GROUND SHOCK-INDUCED MX TRENCH COLLAPSE

Systems, Science and Software, Inc.
P.O. Box 1620
La Jolla, California 92038

18 October 1980

Final Report for Period 27 March 1978—30 April 1979

CONTRACT No. DNA 001-78-C-0211

APPROVED FOR PUBLIC RELEASE;
DISTRIBUTION UNLIMITED.

THIS WORK SPONSORED BY THE DEFENSE NUCLEAR AGENCY
UNDER RDT&E RMSS CODE B344078462 J24AAXYX95516 H2590D.

Prepared for
Director
DEFENSE NUCLEAR AGENCY
Washington, D. C. 20305

Destroy this report when it is no longer needed. Do not return to sender.

PLEASE NOTIFY THE DEFENSE NUCLEAR AGENCY, ATTN: STTI, WASHINGTON, D.C. 20305, IF YOUR ADDRESS IS INCORRECT, IF YOU WISH TO BE DELETED FROM THE DISTRIBUTION LIST, OR IF THE ADDRESSEE IS NO LONGER EMPLOYED BY YOUR ORGANIZATION.

UNCLASSIFIED

SECURITY CLASSIFICATION OF THIS PAGE (When Data Entered)

REPORT DOCUMENTATION PAGE	READ INSTRUCTIONS BEFORE COMPLETING FORM
1. REPORT NUMBER: DNA 5182F	2. GOVT ACCESSION NO.: AD-A095255	3. RECIPIENT'S CATALOG NUMBER:
4. TITLE (and Subtitle): HE SIMULATION OF GROUND SHOCK-INDUCED MX TRENCH COLLAPSE	5. TYPE OF REPORT & PERIOD COVERED: Final Report for Period 27 Mar 78—30 Apr 79
	6. PERFORMING ORG. REPORT NUMBER: SSS-R-79-4016
7. AUTHOR(s): J. C. Baker, H. R. Kratz, K. D. Pyatt, Jr., F. I. Peterson, L. E. Bailey, J. L. Waddell	8. CONTRACT OR GRANT NUMBER(s): DNA 001-78-C-0211
9. PERFORMING ORGANIZATION NAME AND ADDRESS: Systems, Science & Software, Inc. P.O. Box 1620 La Jolla, California 92038	10. PROGRAM ELEMENT, PROJECT, TASK AREA & WORK UNIT NUMBERS: Subtask J24AAXYX955-16
11. CONTROLLING OFFICE NAME AND ADDRESS: Director Defense Nuclear Agency Washington, D.C. 20305	12. REPORT DATE: 18 October 1980
	13. NUMBER OF PAGES: 74
14. MONITORING AGENCY NAME & ADDRESS(if different from Controlling Office)	15. SECURITY CLASS (of this report): UNCLASSIFIED
	15a. DECLASSIFICATION DOWNGRADING SCHEDULE

16. DISTRIBUTION STATEMENT (of this Report)

Approved for public release; distribution unlimited.

17. DISTRIBUTION STATEMENT (of the abstract entered in Block 20, if different from Report)

18. SUPPLEMENTARY NOTES

This work sponsored by the Defense Nuclear Agency under RDT&E RMSS Code B344078462 J24AAXYX95516 H2590D.

19. KEY WORDS (Continue on reverse side if necessary and identify by block number)

MX Trench
Ground Shock-Induced Trench Collapse
Bar Gauges
HE Simulation Experiment

20. ABSTRACT (Continue on reverse side if necessary and identify by block number)

In order to address the problem of energy coupling to an MX trench due to collapse initiated by strong direct-induced ground shock, an HE simulation experiment was defined. The nuclear environment to be simulated was extracted from a detailed calculation of 1 megaton surface burst performed by (S). The range from ground zero for the nuclear surface burst was chosen to be 12.5 m. This results in a peak pressure of 90 Kbar at the trench.

The simulation experiment consisted of a rectangular slab of high-

DD FORM 1 JAN 73 1473 EDITION OF 1 NOV 65 IS OBSOLETE

UNCLASSIFIED

SECURITY CLASSIFICATION OF THIS PAGE (When Data Entered)

Systems, Science, and Software, Inc.

20. ABSTRACT (Continued)

Cont

explosive positioned on the ground surface over a buried trench. The primary instrumentation was high-speed photography to record details of the collapse and time-of-arrival and pressure gauges down-pipe from the region of rapid collapse to define the shock launched along the trench. Pressure in the soil and at the bottom of the trench was also measured. The emphasis of the simulation experiment was on energy coupling rather than pipe flow. A two-dimensional prediction calculation was performed to try to guide gauge settings and timings.

Two pre-shot tests were performed which validated the concept; the main experiment gave good data return. A cross-correlation of the various diagnostics which yielded believable results seemed to confirm the implications of the calculations that strong ground-shock induced trench collapse is not an efficient method for coupling energy down the trench. It is concluded that the off-line burst does not pose a critically stressing environment from a systems design viewpoint.

TABLE OF CONTENTS

LIST OF ILLUSTRATIONS

LIST OF ILLUSTRATIONS (CONTINUED)

LIST OF TABLES

SECTION 1.

INTRODUCTION

The 30-day study group of MX trench testing requirements[1] concluded that strong, direct-induced ground shock resulting from a near-miss nuclear burst is an energy source for trench collapse that is highly uncertain and has a significant impact on the environment definition. Present uncertainties in the modeling of direct-induced ground shock collapse are manifest as order of magnitude uncertainties in the plug pressure environment. The study group further concluded that the data requirement for strong ground shock-induced collapse was not being addressed in the then current MX experimental program, but that this requirement could be met by static HE tests. This report will present the definition of the nuclear environment resulting from a 1 megaton surface burst and the experiment designed to simulate the effect of that environment on an MX trench.

SECTION 2.

BACKGROUND

Systems, Science and Software (S^3) under separate contract had performed a detailed calculation of a 1 MT surface burst dubbed Source 3/5. This calculation used STREAK, which is a multi-material, Eulerian, radiation-hydrodynamic finite difference computer code. The calculation included a detailed description of the source, the nuclear fireball, airblast coupling, and detailed zoning in the shock region--both direct-induced and airblast-induced. This code was used quite successfully in the previous experiments on the underground tests Ming Blade and Husky Pup, which were designed to validate the predictive codes used in energy coupling calculations. Source 3/5 was carried to a final time of approximately 800 μs at which point the airblast was at a radius of approximately 85 meters and had a shock pressure of about 1.3 GPa (13 kbars). Figure 1 illustrates airblast values for a 1 MT surface burst. The curve marked "Max Surface Airblast" is the peak shock value of the blast wave at that time. The curve labeled "Min Surface Airblast" is the relatively constant (in space) value to which the pressure drops behind the shock. Note that at times earlier than 0.1 ms these two curves come together. The well-formed blast wave does not appear until about this time following a 1 MT surface burst. The only data available lie at pressures below 100 MPa (1 kbar).

The calculation was monitored at points corresponding to the top of the MX trench (approximately 1.5 m below the original ground surface) at various radii. Two of these curves are shown as dashed lines in Figure 1. The close-in values (< 5 m) are not of interest to this problem since the question of direct coupling of the nuclear device to a trench was addressed in the underground test Hybla Gold. The 25 m curve on the downside is mostly an extrapolation from the

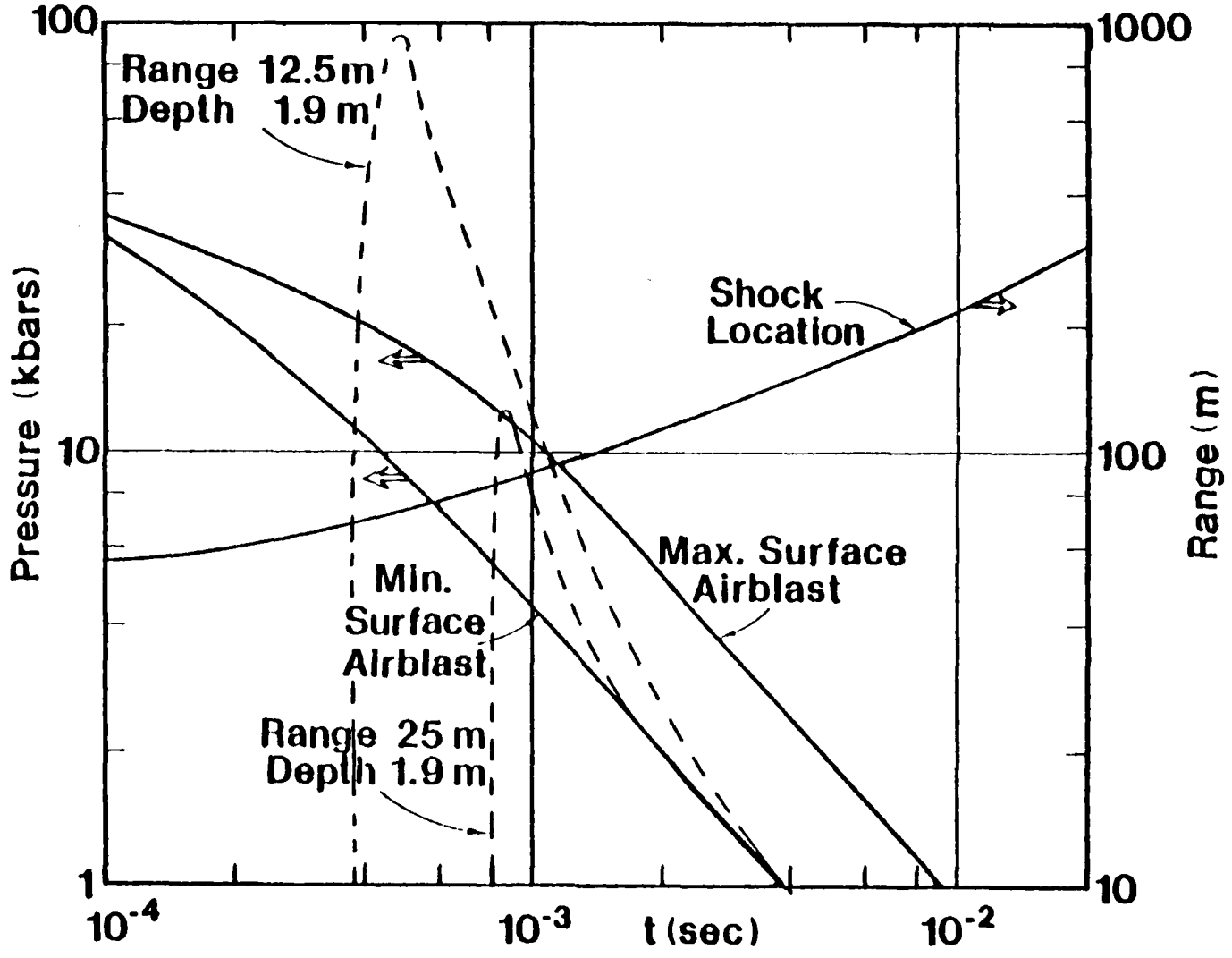

Figure 1. One megaton surface burst.

end of the calculation. This range reaches pressures of approximately 1 GPa (10 kbars), which is lower than values of interest. The 12.5-m range shows a peak pressure of approximately 9 GPa (90 kbars), which is above levels usually available through airblast coupling using HE. Yet this value is in the interesting range for trying to understand how pipe crush will couple energy down the length of the trench.

Turning to Figure 2, in (a) are plotted the 100 GPa (1 mbar) and 10 GPa (100 kbar) isobars. This stress level does not occur at the same time at all locations so this plot is a synthesis of several times. These curves are displaced downward at radii less than 5-10 m because the calculation included a cylindrical room roughly approximating another trench configuration directly under the explosion point. In Figure 2(b), plotted as a solid line, is the pressure at point A in Figure 2(a) as a function of time. The calculated ground shock arrives at the trench 400 μs after detonation, with a peak pressure of 9 GPa. This wave decays to half-value in 200 μs. The highly impulsive load represented by this pressure-time history initiates the collapse of the trench wall at a spall velocity of approximately 0.2 cm/μs. Due to the transient nature of the loading, most of the wall displacement actually takes place after the passage of the waveform. Since the direct-induced ground shock also decays very rapidly with slant range (cf., Figure 2(a)), only about 12 m of the trench are subjected to the very high initial closure velocities. However, airblast-dominated closure continues to pinch off the trench at much lower velocities out to several hundred meters. Admittedly, there are uncertainties in this calculation of the predicted stress field following a 1 MT surface burst, but the calculation does suggest the environment to be simulated to study the energy ultimately coupled to the pipe by the ground shock-induced collapse.

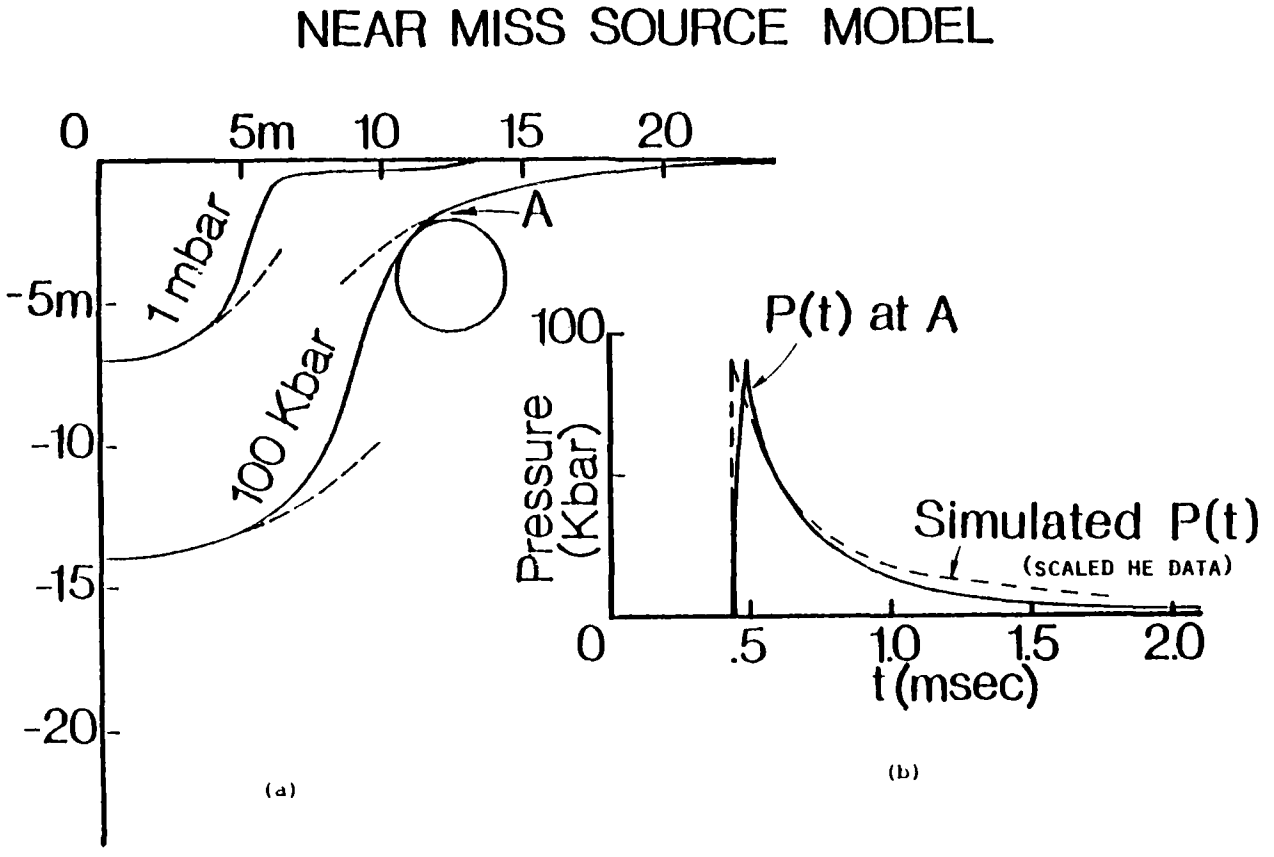

Figure 2. Near miss source model.

Figure 2(b) also illustrates the type of scaled pressure-time history (dashed curve) obtainable from HE coupled directly into soil. The simulation experiment consists of a rectangular slab of HE positioned over a buried trench. Calculations indicate that this source is capable of inducing a 9 GPa shock at the trench wall. Moreover, the correct pressure-time history at this point can be achieved by adjusting the thickness of the HE slab. (The decay of pressure with depth will not be the same in the HE case as in the nuclear, but the nuclear calculation has not been carried to the point where the shock has totally traversed the trench location. From earlier data, it appears that the nuclear value might reach about 2.5 - 3.0 GPa at the trench bottom and the HE case about 1.5 GPa.) The simulation experiment was conducted with a 1/16th-scale trench. Table 1 lists some parameters of the HE necessary to obtain the correct P(t). The slab is approximately 1.2 m square by 6.93 cm thick (Composition C-4 with a total mass of 166 kg). (This is about the maximum surface charge which can be fired at the S^3 Green Farm test site.) The areal size of the slab is dictated by efforts to avoid any edge effects affecting the ground shock until the wave has passed below the bottom of the trench.

TABLE 1

1/16 SCALE EXPERIMENT

HE slab thickness	6.93 cm
Depth of pipe burial + wall thickness	7.62 cm + 2 cm
HE mass (1.2 m x 1.2 m)	166 kg

In order to prove the concept and get ideas for timing settings on scopes in the main experiment, two pre-shot tests were performed. These tests were mainly to check out the optics, framing camera and argon candle performance. Commercial 15.24 cm (6 in) concrete pipe and scaled HE charges were used. The first test indicated that careful alignment of all the optics was absolutely essential for obtaining pictures of high enough quality to analyze. The second pre-shot test used the same scaling as the first, but the inside of the pipe was coated with a black, non-reflective material. Opal glass was placed over the argon candle to get uniform illumination of the pipe cross-section and more than a day was spent in aligning the mirrors and the pipe.

A STREAK prediction calculation for the full-scale experiment was performed to determine if there were any potential problems with the design. This was done in X-Y plane geometry, taking a cross-section of the pipe, soil, and charge. Main variables of interest were pressures in the air as the pipe squeezed off and stagnation pressures at the bottom of the pipe. This calculation did not include either radiation or strength, since neither was significant for this problem. The code used tracer particles to delineate material boundaries, and these boundaries will be shown in following figures. Both the inside and outside boundaries of the pipe will be presented in the tracer plots and will be compared with the photographs taken during the second pre-shot test described above. The calculated times will be scaled to the actual times for this particular event. Composition B-3 JWL equation-of-state coefficients were used in the calculation.

Figure 3 is the first of a series of plots comparing the event and the code. On the left (Figure 3(a)) is a series of photos taken down the pipe while the collapse was in progress. There are 7.63 μs

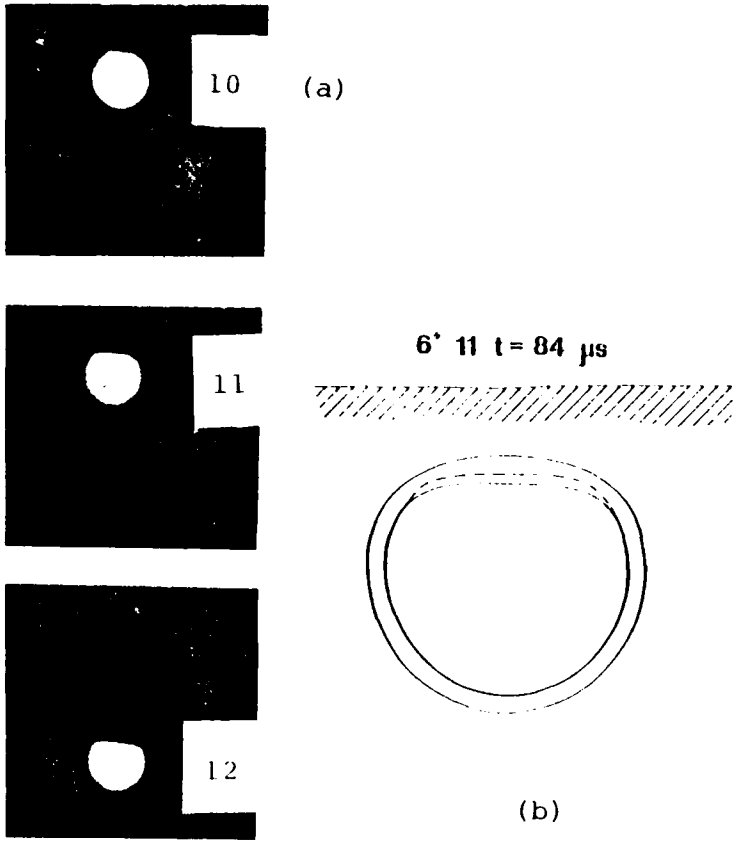

Figure 3. Experimental/calculational comparison for 15.24 cm (6-in) diameter pre-shot test at 84 μs.

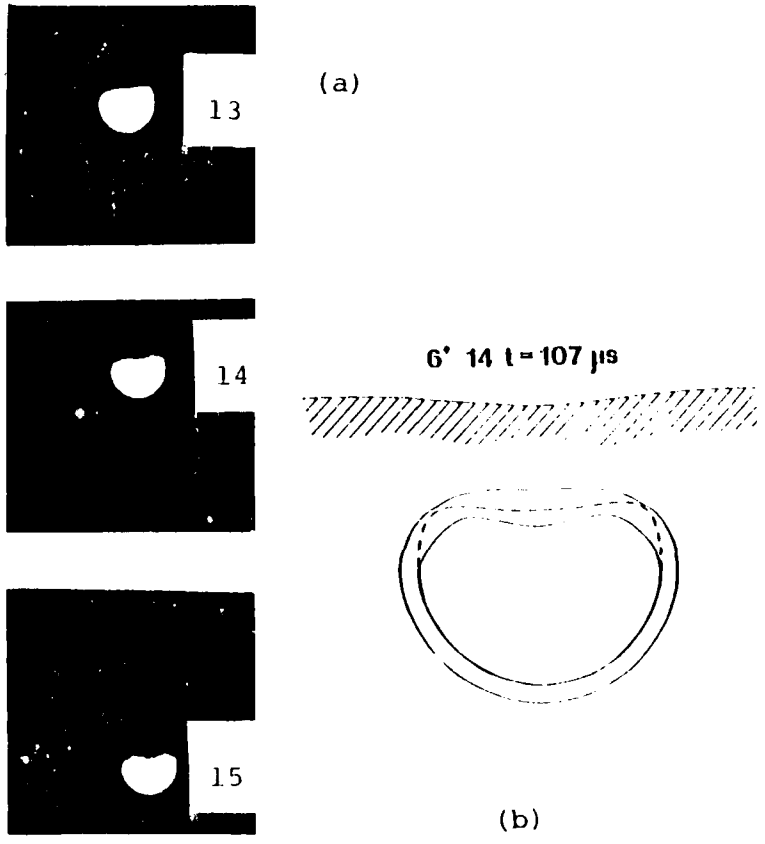

Figure 4. Experimental/calculational comparison for 15.24 cm (6-in) diameter pre-shot test at 107 μs.

between frames and the collapse started at about Frame 9, which is not shown. To the right (Figure 3(b)) is an artist's rendition (dashed line) of the pipe shape at the central frame of the three presented. The heading indicates the 15.24 cm experiment, Frame 11, at a time of 84 μs from detonation of the main HE charge. The quality of reproduction is not good enough to show the sharp boundary between the air and the pipe wall, apparent in the original photos. Figure 3(b) also shows the calculated configuration overlaid on the photo rendition. The shape is remarkably similar and the location is in reasonable agreement. (The calculation used an equation-of-state for alluvium at normal density approximately 2.1 gm/cm^3 rather than sand at a density of approximately 1.6-1.7 gm/cm^3 as in this experiment.)

Figure 4(a) and 4(b) make the same comparison at 107 μs, Figures 5(a) and 5(b) at 130 μs, Figures 6(a) and 6(b) at 153 μs, Figures 7(a) and 7(b) at 176 μs, and Figures 8(a) and 8(b) at 199 μs. In all of the photos there is no indication of a break-up of the pipe-wall/air interface. The calculation is in qualitative agreement with the observed behavior, although it is protruding more on axis. This is thought to be due simply to coarse zoning problems in the regions of the developing lobes. The lobe effect was not expected when the calculation was performed and thus was not adequately accounted for in the problem set-up. The air in these lobes reaches a calculated maximum pressure of no more than about 100 MPa (1 kbar), which may not be effective in driving a strong shock down the length of the tunnel.

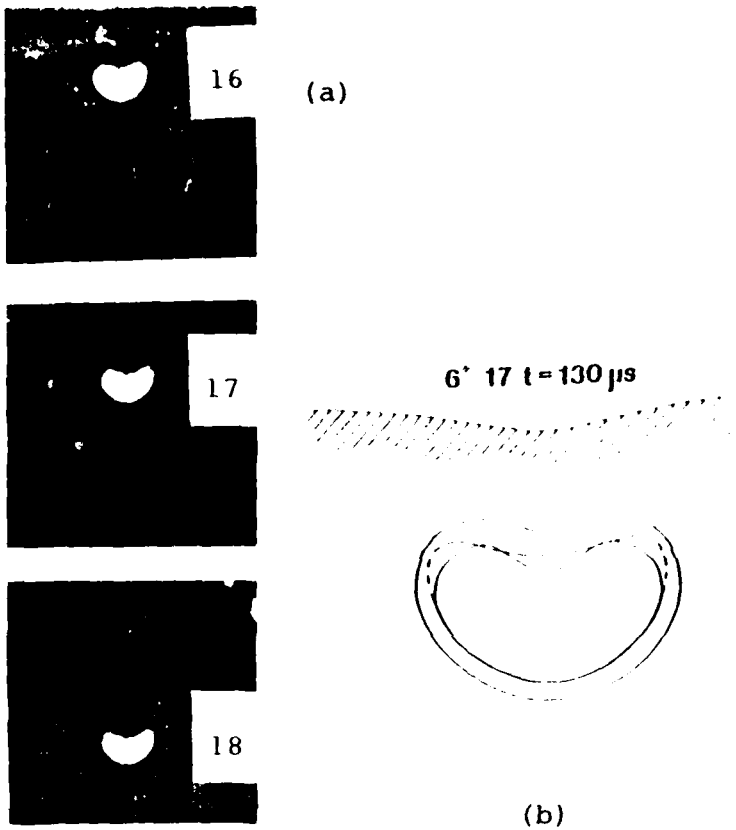

Figure 5. Experimental/calculational comparison for 15.24 cm (6-in) diameter pre-shot test at 130 μs.

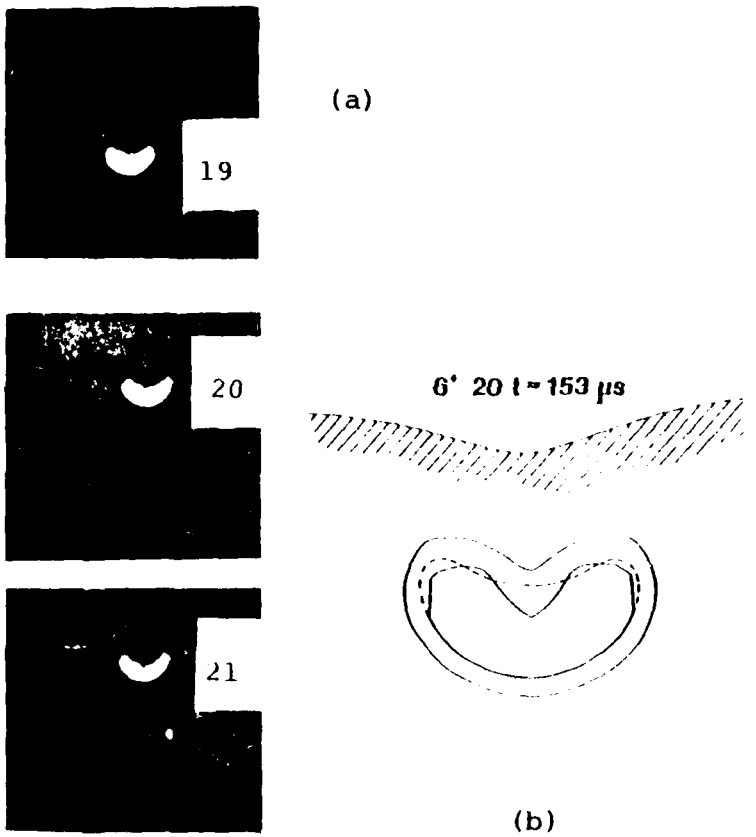

Figure 6. Experimental/calculational comparison for 15.24 cm (6-in) diameter pre-shot test at 153 μs.

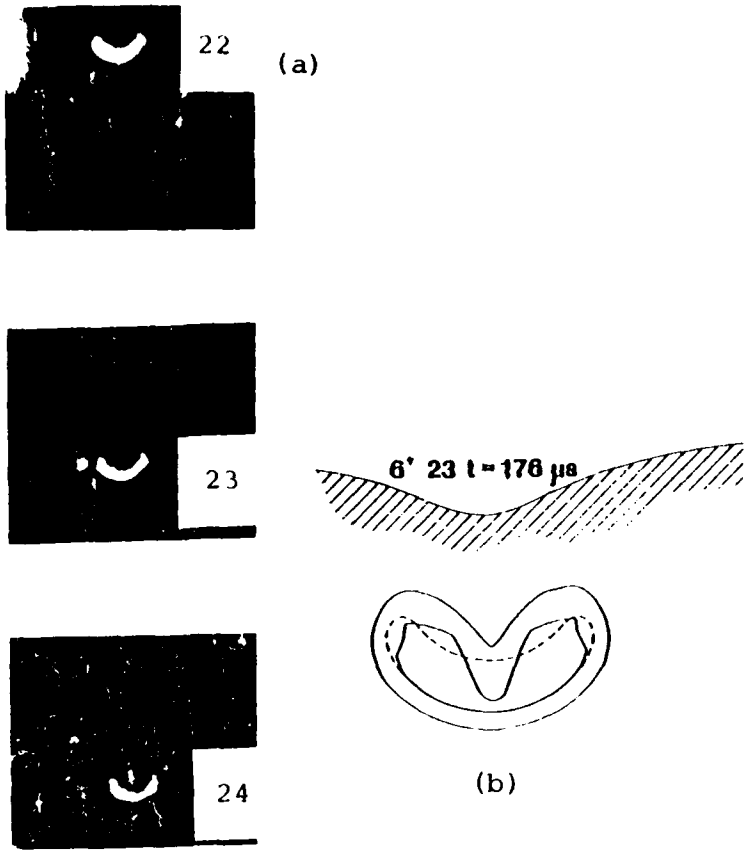

Figure 7. Experimental/calculational comparison for 15.24 cm (6-in) diameter pre-shot test at 176 μs.

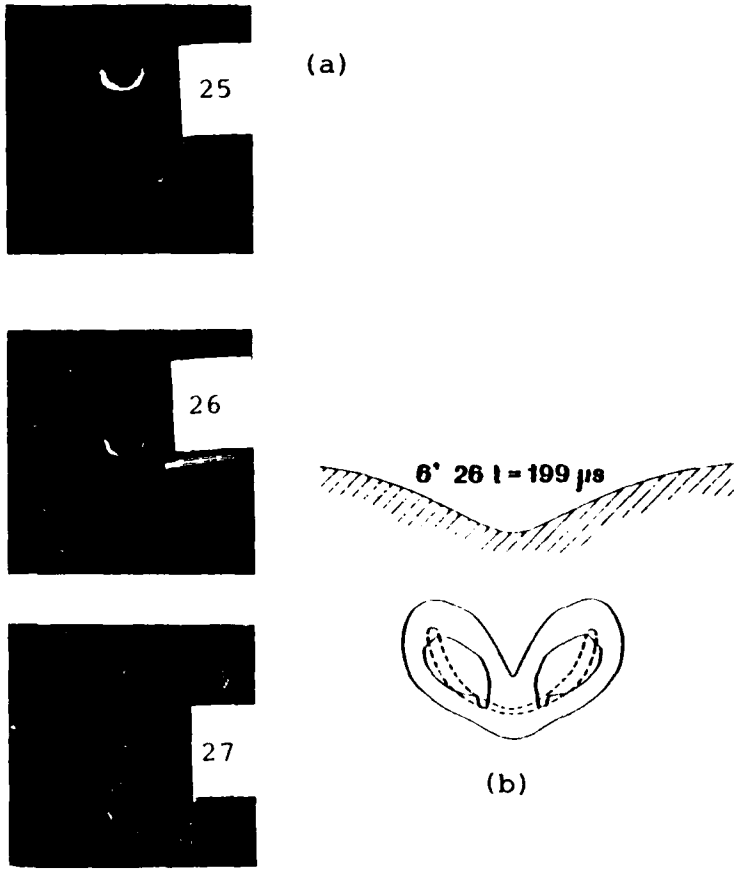

Figure 8. Experimental/calculational comparison for 15.24 cm (6-in) diameter pre-shot test at 199 μs.

SECTION 3.

MAIN EXPERIMENT DESIGN

The scaled trench for the main experiment is a concrete pipe 26.5-cm ID with a 2-cm wall, 10 m long (see Figure 9). The pipe depth of burial (7.62 cm - see Table 1) corresponds to a 4-foot burial full-scale, rather than the 5 feet proposed for an MX trench, but since the chief concern is energy coupling by the collapse to the remainder of the pipe, this is not a serious difference. Since concrete pipe with walls this thin is not available commercially, the pipe was cast by S^3 in sections about 72 cm long in specially built forms. These forms consist of two coaxial Burke tubes, one 26.67 cm OD and the other 30.48 cm ID. The main problem in casting the pipes, which are 30.48 cm OD with 1.91 cm wall, was the elimination of voids in the cast concrete. This was accomplished by the combination of addition of Plastiment, a retardant and air deentraining agent, to the concrete mix and very thorough vibration of the concrete after filling the forms. Four vibrators were used, one each on the bottom and top collars of the form, one in the concrete mix itself and the fourth on the outside of the form, moving it gradually from the bottom to the top of the form. In addition to the vibrators, the forms were mounted on a shake table during filling. This procedure eliminated nearly all voids in the concrete; the few remaining small voids were filled before installing the pipes in the experiments. The forms were removed 24 hours after pouring and curing continued by submerging the pipes in water for an additional 4 or 5 days.

The pipe was mounted in a trench which was then back-filled with Overton sand. Figures 10(a) and (b) illustrate the set-up before the sand was filled. Figure 10(b) also illustrates the

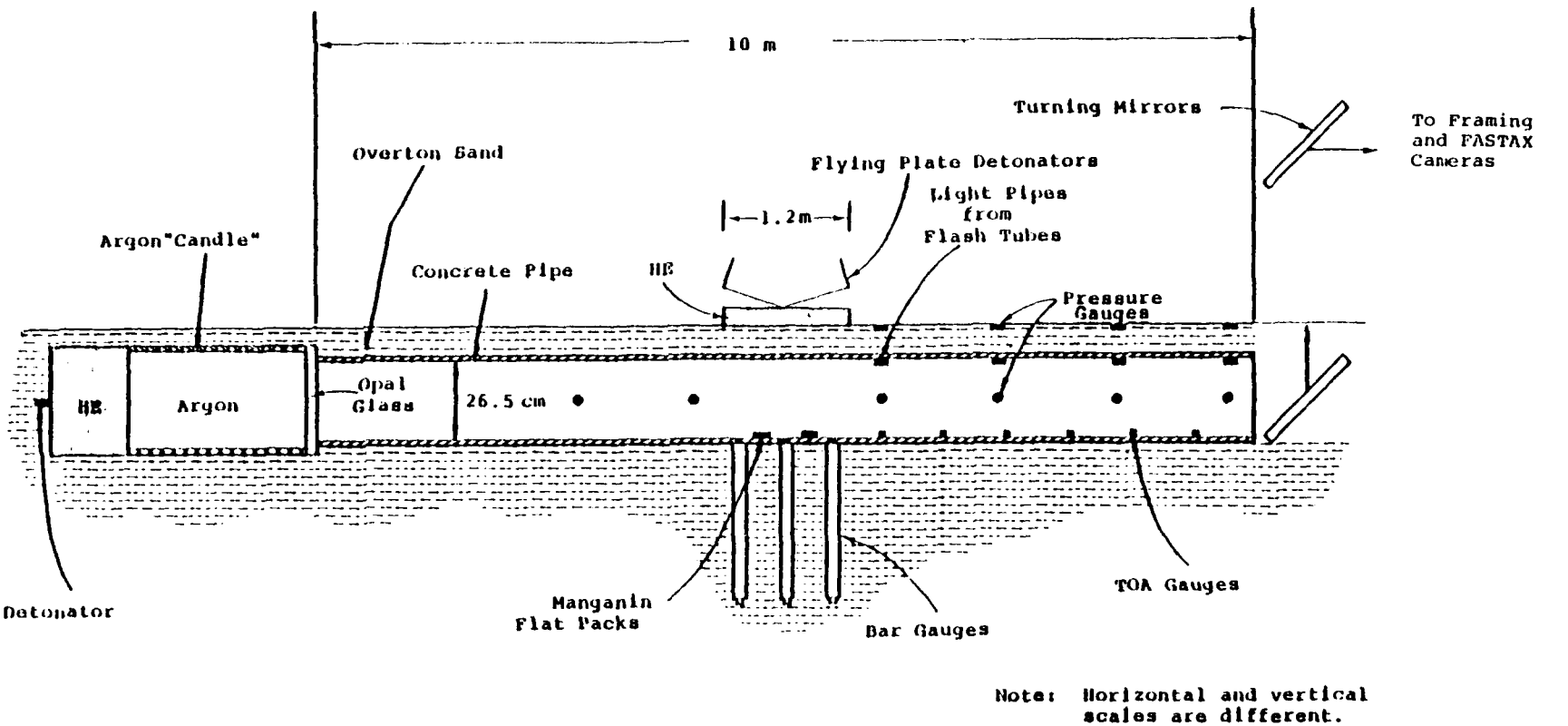

Figure 9. Experimental setup.

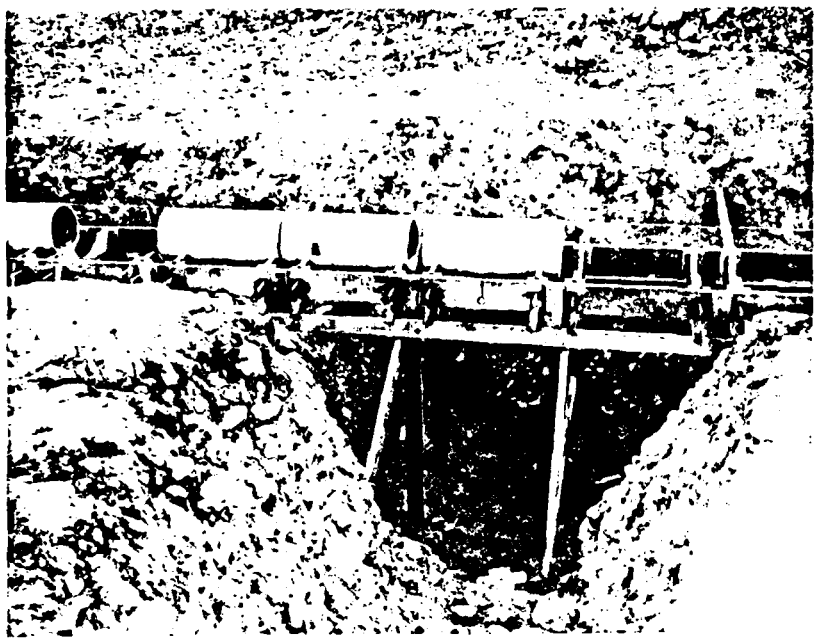

(a) Mounted pipe in trench over excavation for bar gauges.

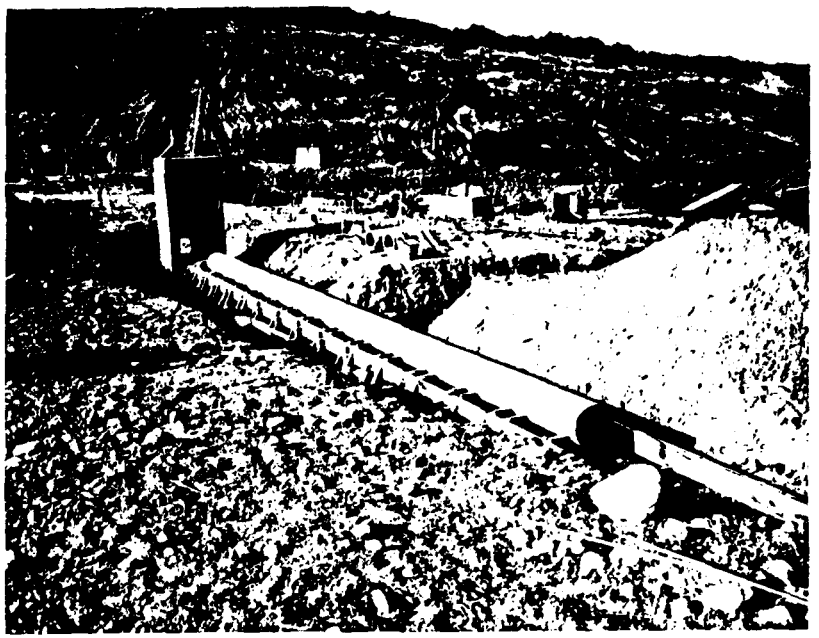

(b) Turning mirror frame and complete pipe.

Figure 10. Setup before sand filled.

turning mirror frame indicated schematically in Figure 9. Overton sand (60 mesh) was chosen as the soil material rather than alluvium because of the necessity to pack the material around the pipe with a relatively uniform density, which appeared all but impossible for alluvium. A special technique of "raining" the sand into the trench had to be developed to insure high, uniform density. Sand was fed into a hopper and a continuous blast of air from a fan picked up individual grains at the bottom of the hopper and rained them over the area to be covered (see Figures 11(a) and (b)). This allowed the grains to pack more tightly and uniformly to a measured bulk density of 1.743 gm/cm^3. Samples were measured during the process to assure consistency.

The HE charge was positioned on the surface of the sand directly above the center of the pipe as shown in Figures 9 and 12(a). The HE charge was detonated by planar impact over its entire surface with two flying-plate type plane wave initiators (see Figure 12(b)). Visible in Figure 12(b) is one of the line wave generators which was detonated at the top apex of the triangle. The line wave generator initiates the upper edge of the sheet of explosive over the flyer plate, sending the flyer plate into planar impact with the large HE pad. It should be appreciated that this generator is about 4 feet wide, which is significantly larger than most previous efforts, which have been about one foot or less. The flyer plate angle, dimensions and explosive thickness and configurations were developed and tested in a series of experiments with time-of-arrival gauges. These tests suggested that the HE charge would be planar initiated with $\pm$ 3μs.

The large wooden structure in Figure 12(b) is a dirt-filled canopy over the explosive designed to reduce noise and airblast effects in nearby residential areas. (The sheet of plywood covering the foreground of the test bed was removed before the test.)

(a) Sand fed into hopper.

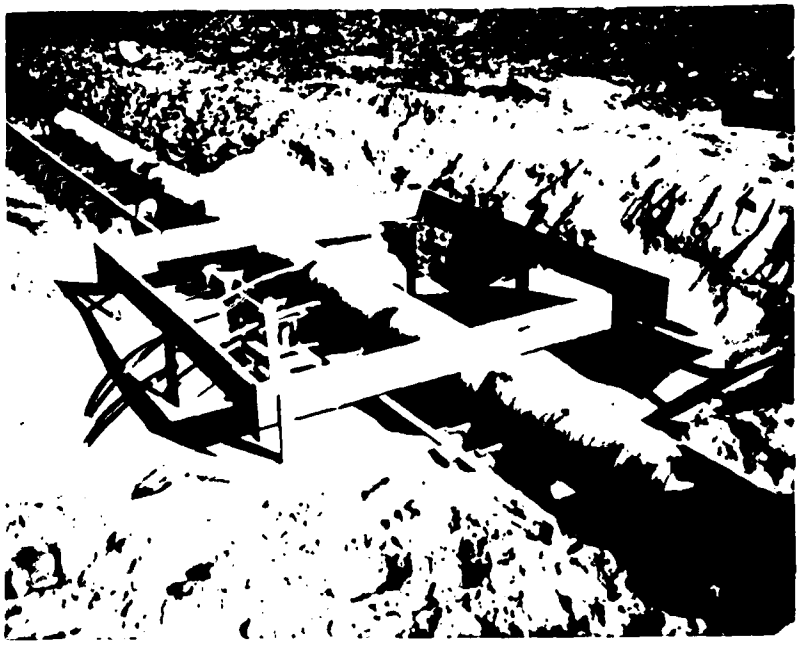

(b) Area "rained with Overton sand.

Figure 11. Raining of sand into trench.

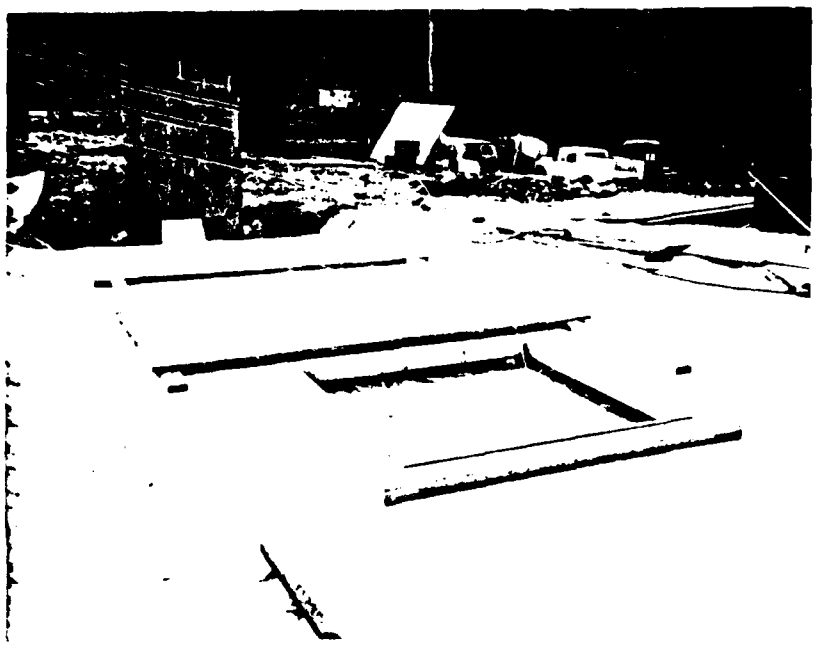

(a) Frame for HE charge positioned on surface of sand directly above center of pipe.

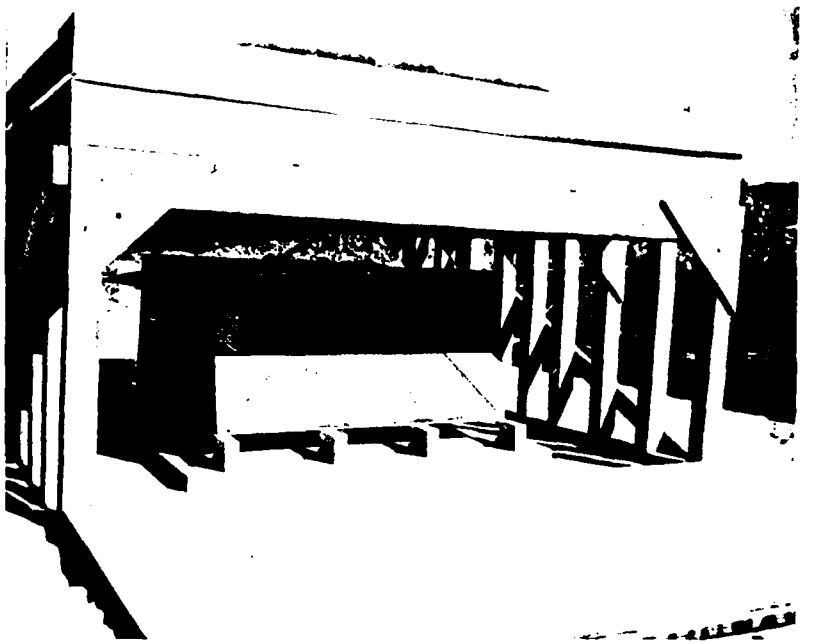

(b) Completed setup with line and plane wave generators visible.

Figure 12. Views of explosive setup.

The main diagnostic to measure the rate and shape of the pipe collapse was high-speed photography, using a framing camera running at about 5 μs per frame. The camera looked directly down the axis of the pipe via the turning mirrors mentioned above. The pipe was back-lighted from the opposite end with an explosively driven argon "candle," the length of which (3.05 m) was great enough that the shock wave did not arrive at the end of the candle until after the collapse of the pipe was complete. What was actually photographed was a shadow-graph of the collapsing pipe directly under the HE charge. In this way, both the rate of collapse and the cross-sectional shape of the collapsing pipe were determined. An opal glass window at the end of the argon candle was found to produce much more uniform backlighting than a transparent window. Figure 13(a) shows the candle before being lowered to line up with the pipe and being buried. Figure 13(b) is an overview of the test bed with the candle being buried at the far end. The bunker is off to the left in this view.

As indicated in Figure 9, various gauges were used to measure pressure and time of arrival in the pipe, in the soil, and on the ground surface above the pipe. The three bar gauges (tungsten-aluminum with quartz crystals as transducers) shown were to measure the air pressure directly under the collapsing portion of the pipe. (A general discussion of bar gauges may be found in Reference 2.) In addition to these gauges, two more bar gauges were located in the center plane perpendicular to the pipe axis, but at an angle of 20 degrees to the vertical (see Figure 14). The purpose of these gauges was to measure the air pressure in the lobes which might form (as suggested by the calculation and the pre-shot test) on either side of the axis during pipe collapse. The manganin flat packs on the bottom of the pipe under the HE charge were to measure the pressure produced by the impact of the collapsing upper portion of the pipe wall on the bottom of the pipe. Five manganin gauges in

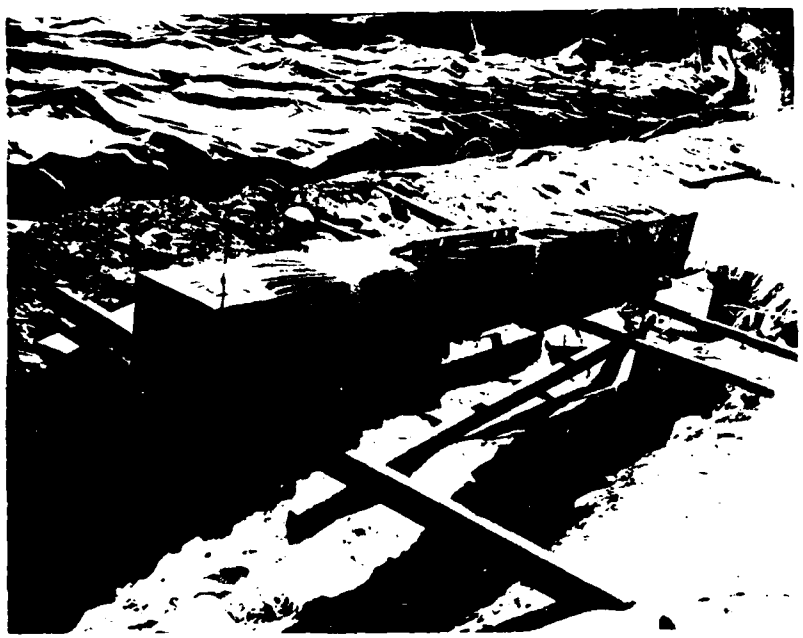

(a) Argon candle before being lowered.

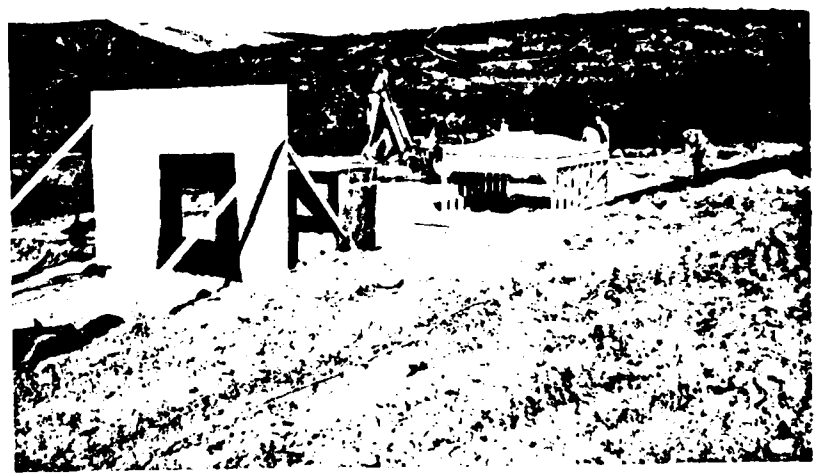

(b) Overview of test bed with candle being buried at far end.

Figure 13. Candle being lowered into test bed.

14 (a) Below-pipe view of the five bar gauges.

14(b) Schematic cross-section of test bed.

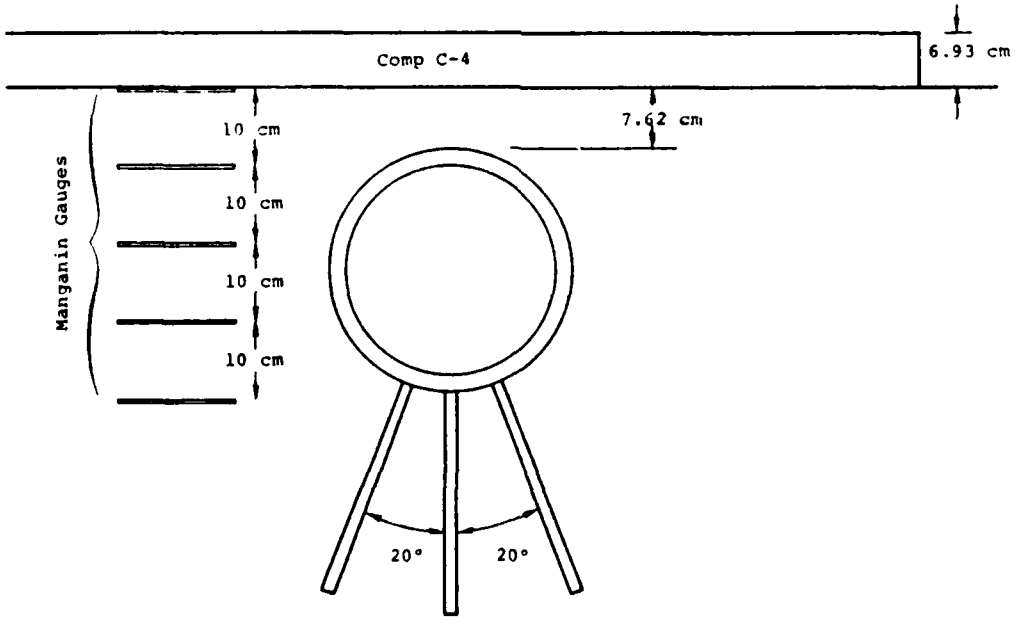

Figure 14. Gauge setup.

steel flat packs were also distributed in the sand at various distances below the HE charge to measure the ground shock incident on the pipe (see Figure 14).

Time-of-arrival (TOA) and pressure gauges were located along the inside of the pipe but outside the region of the HE charge to measure the time of arrival and magnitude of the pressure pulse driven down the pipe by the collapse. The TOA gauges were standard PZT-type piezoelectric crystals in pin probes mounted to the pipe wall in Bi-wax plugs cast in place for acoustic isolation. The crystal probes consisted of a simple sandwich of copper foils cemented to each face of the crystal with the sandwich encased in copper foil as an electrical shield. In preliminary tests these probes yielded signals with no measured delay in their onset and about a microsecond rise time at overpressures as low as 25 psi. Additional gauges on the ground surface above the pipe were to measure the airblast incident on the ground outside the HE charge. These pressure gauges (and those down the inside of the pipe) were low-pressure quartz-element gauges similar to the standard Gulf Radiation Technology type, but designed and built by S^3 to be effective at the lower pressures expected (10 - 1,000 psi) in this experimental use. They consisted of a 0.953 cm diameter crystal element in a 1.27 cm thick case. Low noise cable was led out through protective stainless steel tubing to isolation amplifiers which had a gain factor of 5. In preliminary testing, these gauges worked acceptably.

As shown in Figure 9, bundles of light pipes were mounted at various positions along the top inside of the pipe. These light pipes lead to flash tubes which were located beyond the end of the concrete pipe. The ends of the light pipes in the concrete pipe were pointed towards the turning mirrors and were to be photographed

by a remotely controlled Fastax camera. The purpose of this arrangement was to measure the rate of collapse of the pipe outside the rapid closure region under the HE charge.

This completes the summary of the instrumentation of the test bed. Table 2 lists the experiments, the method employed and the number of gauges.

TABLE 2

SUMMARY OF EXPERIMENTS IN TEST BED

	Experiment	Equipment	Number of Experiments
1.	Pipe collapse in rapid closure region	Framing camera	1
2.	Pipe collapse outside rapid closure region	Rastax camera Light pipes	1 4
3.	Air pressure versus time at the bottom of the trench in rapid closure region	Bar gauges	3
4.	Air pressure versus time in lobe region of collapse	Bar gauges	2
5.	Impact pressure versus time at the bottom of the trench	Manganin gauges	2
6.	Free-field pressure versus time in the soil under the HE	Manganin gauges	5
7.	Air pressure versus time in pipe outside rapid closure region	Quartz gauges	4 down-pipe 2 up-pipe
8.	Air pressure versus time on surface outside rapid closure region	Quartz gauges	4
9.	Time-of-arrival of pressure wave in pipe outside rapid closure region.	PZT pin probes	4

SECTION 4.

RESULTS

The experiment was detonated 9 December 1978 at the S^3 Green Farm test site. The most complete results were from the framing camera, the bar gauges, and the time-of-arrival gauges. These measurements were sufficient to define the coupling efficiency down-pipe from the HE charge. The Fastax camera had its film break early at about 75 feet and there was no record of the pipe collapse outside the rapid closure region. Few of the quartz gauges had any useful information. The manganin gauges gave data that cause confusion in interpretation. The data from the various experiments are discussed below. Figures 15(a) and 15(b) are post-shot views of the test bed.

4.1 PIPE COLLAPSE IN RAPID CLOSURE REGION

Based on the pre-shot prediction calculation and limited by the number of frames (80) available on the framing camera, it was determined to run the camera at about 5 μs/frame. Since the predicted pipe collapse duration was ~ 220 μs, this would give 44 frames to define the behavior of the top surface. The actual speed of the camera was 4.93 μs/frame as shot. The camera had to start early enough to record the turn-on of the argon candle which allows absolute timing to be set. All times to be reported will be referenced to time zero being the start of detonation of the line wave generator (console zero). Figures 16, 17 and 18 are the photo record of the collapse (frames 4-9 are deleted since there was no motion during that interval). Frame 1 on Figure 16 is the turn-on of the argon candle (previous frames were all dark) and this was at a time of 205 μs as noted. The small identations at the equator and

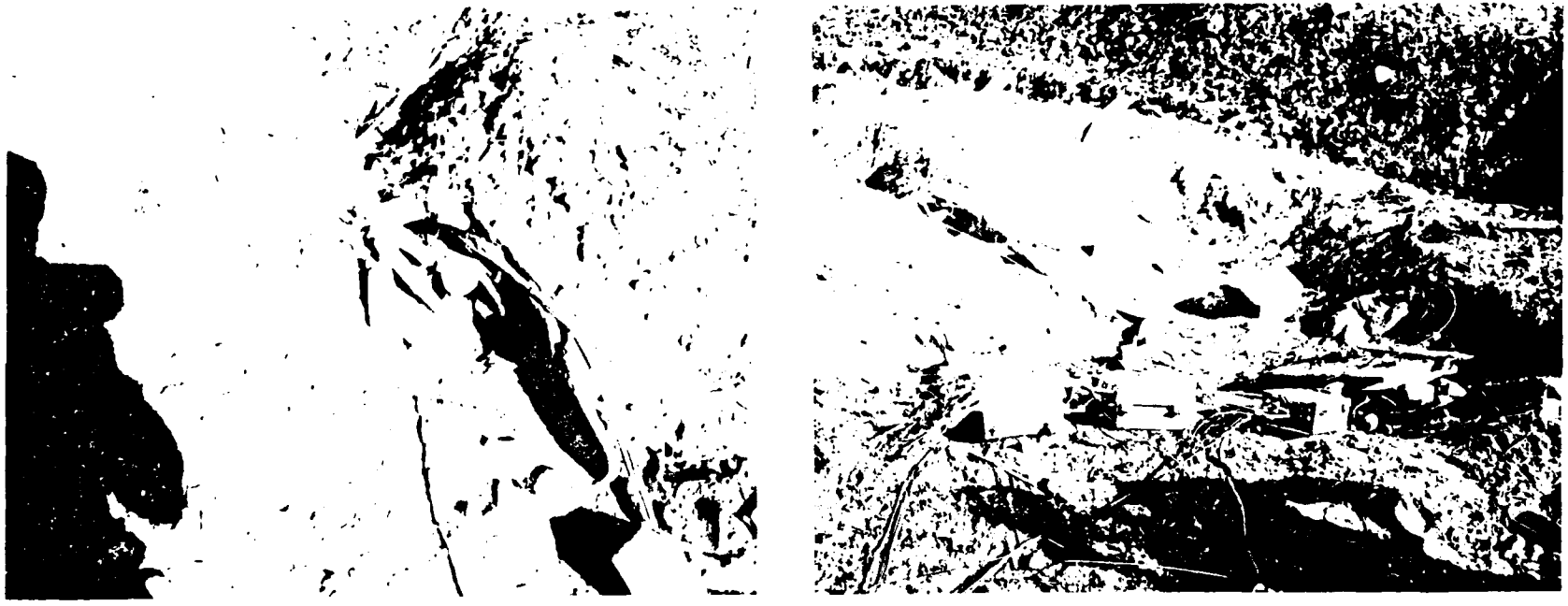

(a) Pipe fragments following shot. This section of the test bed was between the HE charge and the argon candle.

(b) Center of test bed showing crater and some experimental electronics.

Figure 15. Post-shot views of test bed.

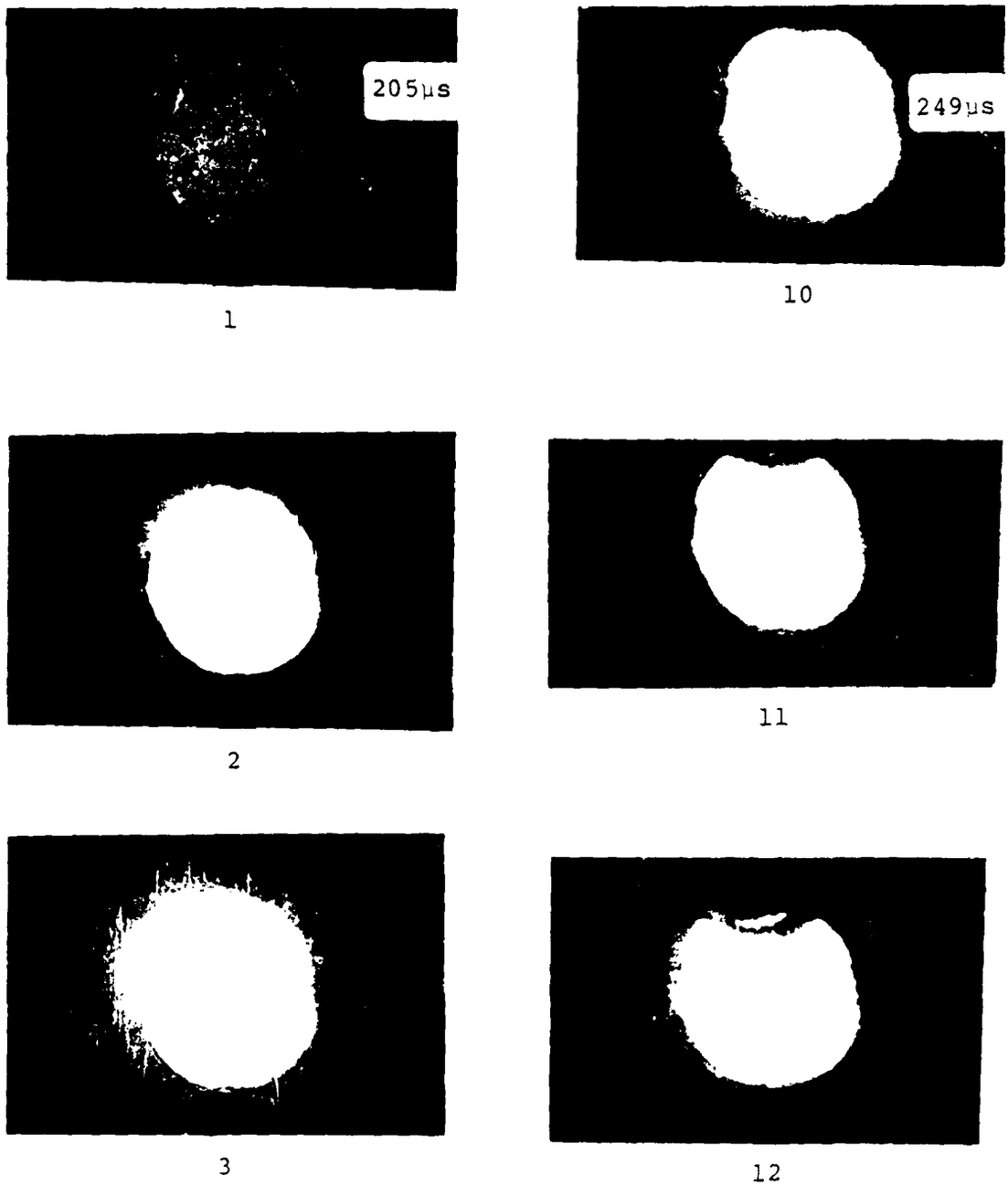

Figure 16. Framing camera photos of pipe blow-in (4.93 μs between frames). Frame (1) shows candle turn-on and frame (10) shows first detectable motion.

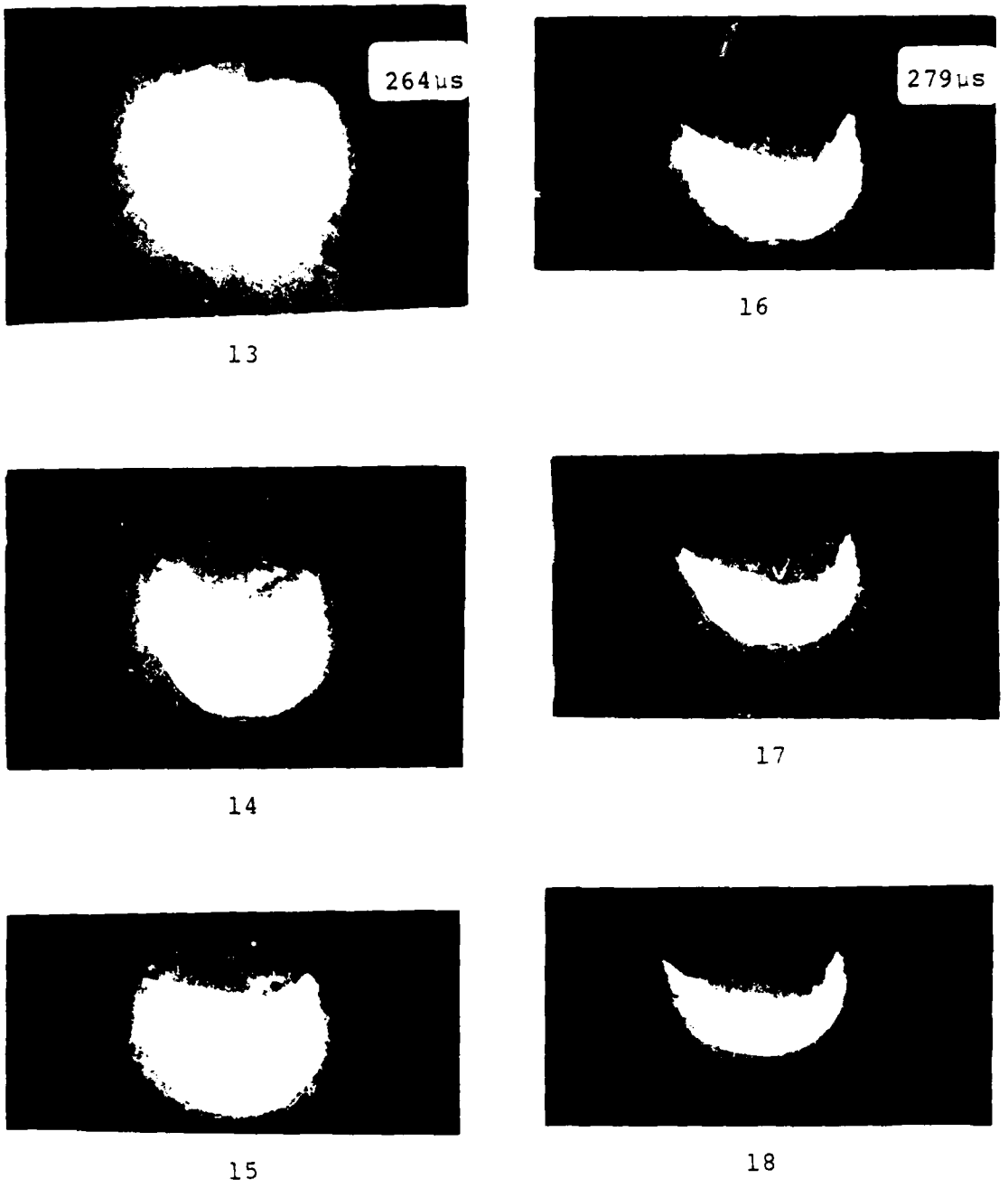

Figure 17. Framing camera photos of pipe blow-in showing low-density material obscuring candle.

19

22

20

23

21

Figure 18. Framing camera photos of pipe blow-in and complete obscuration of candle at 314 µs.

poles are due to cable bundles from in-pipe experiments coming out the end of the pipe. There is a slight oblateness to the image which was caused by inexact alignment and imperfect mirrors.

The first detectable movement occurred at frame 10 at a time of 249 μs. From subsequent motion it would appear that first motion occurred at 248 μs, 24 μs following predicted completion of the HE burn at the surface. (This is to be compared with the predicted interval of 24.7 μs from the calculation, which used an equation-of-state for a different soil material than that actually employed.) The first wisps of material reach the bottom of the pipe in frame 21 (Figure 18) and completely block out the light by frame 23 at a time of 314 μs. This corresponds to a closure velocity of ~ 4×10^5 cm/sec for the material sufficient to block light. The calculated closure (and that observed in the pre-shot test) was ~ 1.2×10^5 cm/sec, over a factor of 3 lower than that observed. Unlike the pre-shot test presented above, there is definite evidence that in this experiment the pipe wall is breaking up under the impulse. Figure 19 is an enlargement of frame 20 showing tendrils of material reaching out. Insufficient light is transmitted to allow a determination to be made of the velocity of the higher density material. This first-impact material is interpreted as being very low density blow-off spalled off the inner surface of the pipe (but adequate to block the light path). The pressure versus time records from the bottom of the pipe (to be presented later) show four (and perhaps 5) distinct impacts (with associated pressures) and this allows us to infer the density of this initial material. The initial pressure pulse in 0.4 kbars which yields a density of ~ 0.003 gm/cm^3 for the first blow-off.

Differences in this experiment from the pre-shot test (which showed no such effect) are chiefly just two: (1) thinner pipe wall

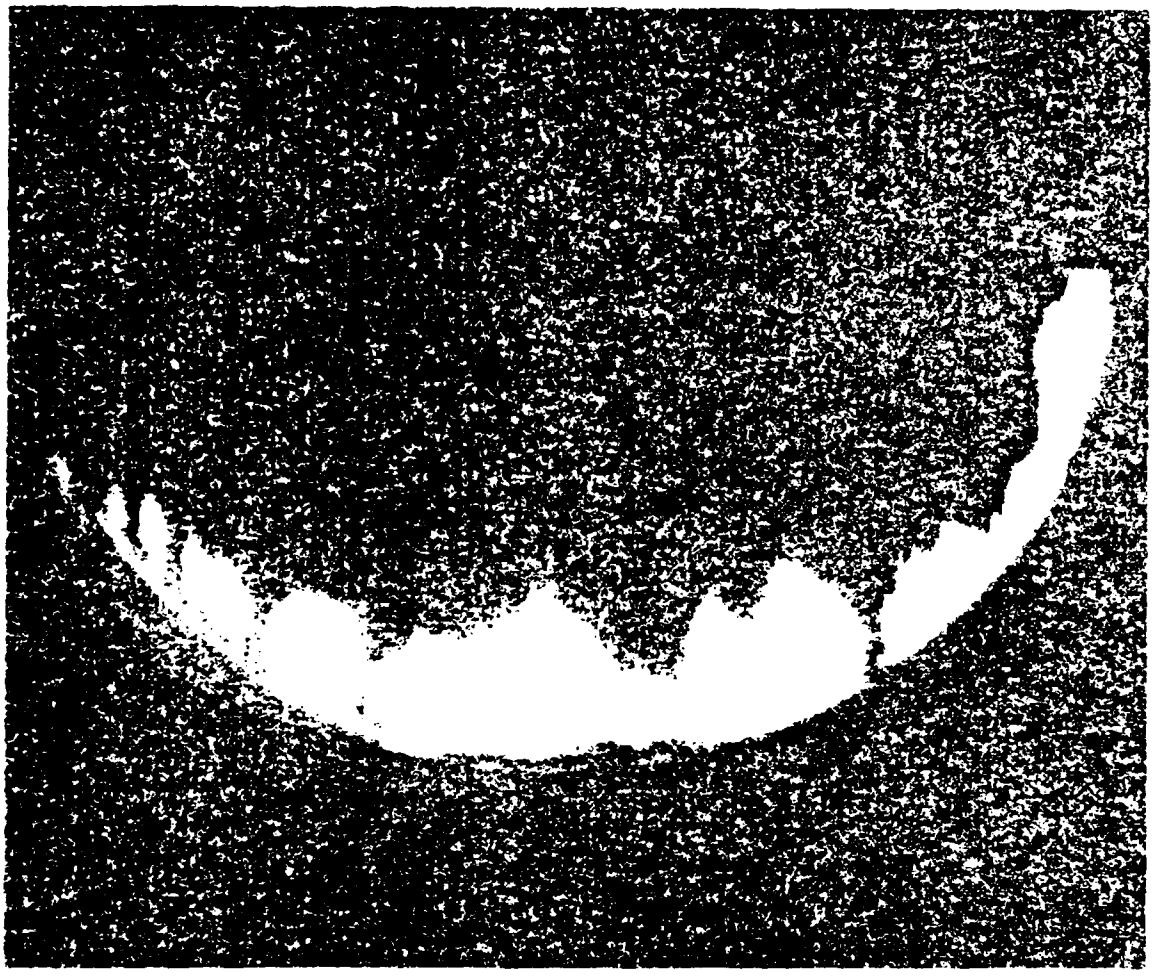

Figure 19. Frame 20 at a time of 299 μs.

and (2) higher ambient density of sand between HE and pipe. (This latter effect manifested itself in another way--following the main shot the area was littered with chunks of a welded Overton sandstone formed by the shock traversing the sand. One further difference was the fact that there were two joints in the pipe under the HE for the main test and none for the pre-shot tests. The low density blow-off material may relate to the joint filler. The lobes observed in the collapse region in the pre-test trials were not observed in the main event because the low density blow-off obscured any observation of the main collapse.

The dominant pressure is reached about 200 μs after first motion, implying the majority of the mass is moving at ~ 1.3×10^5 cm/sec, close to the predicted value. While the optical data only related to the low density blow-off, our experience in the pre-shot test and analysis of the pressure-time histories for the gauges at the bottom of the pipe allowed us to infer the closure configuration.

4.2 PIPE COLLAPSE OUTSIDE RAPID CLOSURE REGION

As indicated earlier, the film in the Fastax camera broke early before the camera reached full speed and there was no record.

4.3 AIR PRESSURE VERSUS TIME AT THE BOTTOM OF THE TRENCH

Three bar gauges were inserted along the centerline of the trench to measure air pressure. Since the pipe roof broke up in closing there was no clearly defined compression of the air in the trench below the HE charge. Instead, the bar gauges measured the stagnation of the blow-off material as it impacted the bottom of the

pipe. Figures 20 through 22 show traces (oscilloscope and tape recorder) for the three gauges below the charge, and the readings are summarized in Table 3. It will be noted that the three gauge records are in very good agreement. Figure 20(a) shows the first impact in the low-pressure range, and Figure 20(b) relates these low-pressure results to the main impact occurring later. This impact, yielding a pressure of ~ 24 kbar on stagnation, is in good agreement with the calculated stagnation which was at ~ 20-30 kbars, but at a somewhat later time (~ 470-480 μs with this fiducial).

The first pressure pulse on all three gauges occurs at about 320 μs. Referring to Figure 18, we would expect a signal starting about 300 μs, if the collapse we are viewing is occurring directly over the bar gauges. The observed closure may be material from the pipe joints that is ahead of the other material and not directly over the bar gauges.

Marked on Figure 20(a) is a plateau following the third impact which might be the measurement of the air in the pipe compressed by the ceiling collapse. It is at a level of ~ 0.6 kbar, while the calculation had suggested ~ 1 kbar. The different mode of collapse could certainly account for this difference. If this speculation is true, it would indicate that although the pipe wall did fractionate, the general features of the collapse could be treated as though the wall retained its integrity as in the pre-shot test.

4.4 AIR PRESSURE VERSUS TIME IN LOBE REGION OF COLLAPSE

Two bar gauges were placed at an angle of 20 degrees to the vertical under the center of the pipe covered by the HE (see Figure 14). Similarly to the 3 gauges along the vertical, there were four

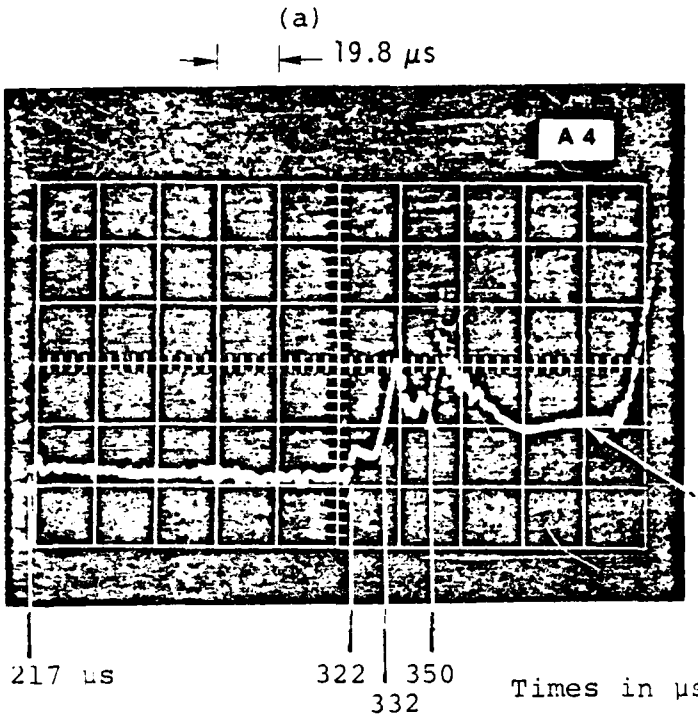

Figure 20. Gauge Qb-2.

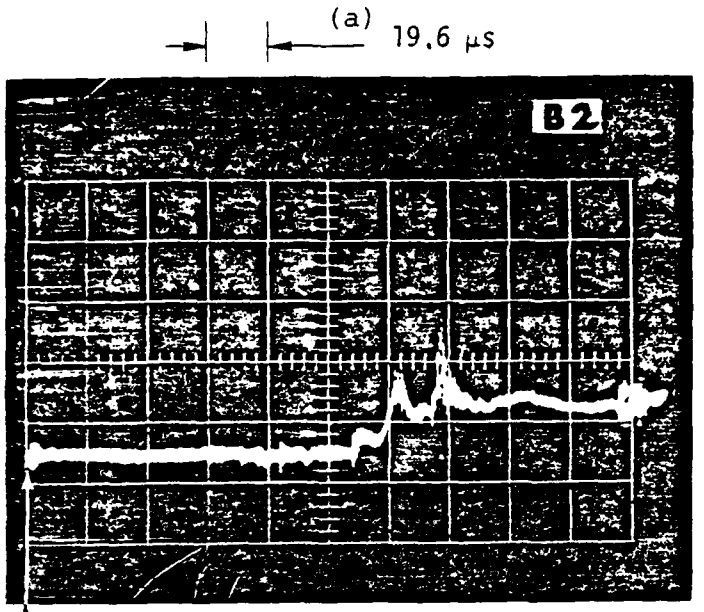

Sweep 19.6 µs/cm

1.12 kbar/cm

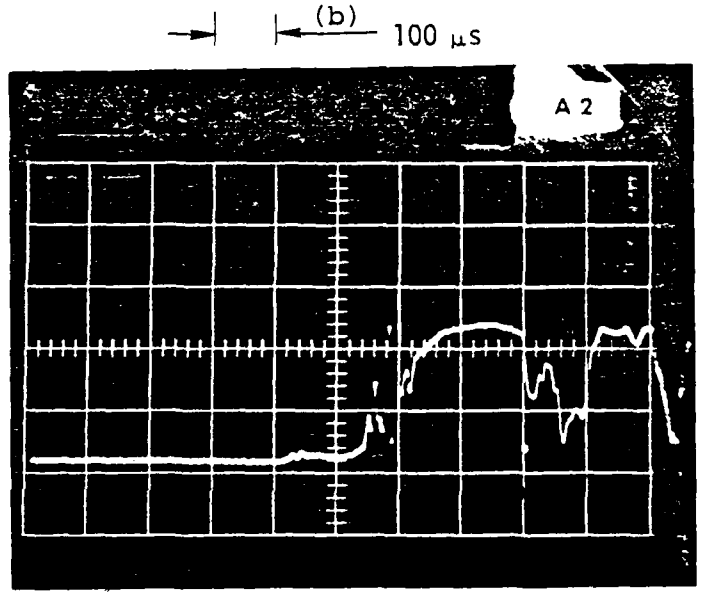

Sweep 100 µs/cm

(+44 µs)

11.1 kbar/cm

(Bar delay 133 µs)

Figure 21. Gauge Qb-3.

(a)

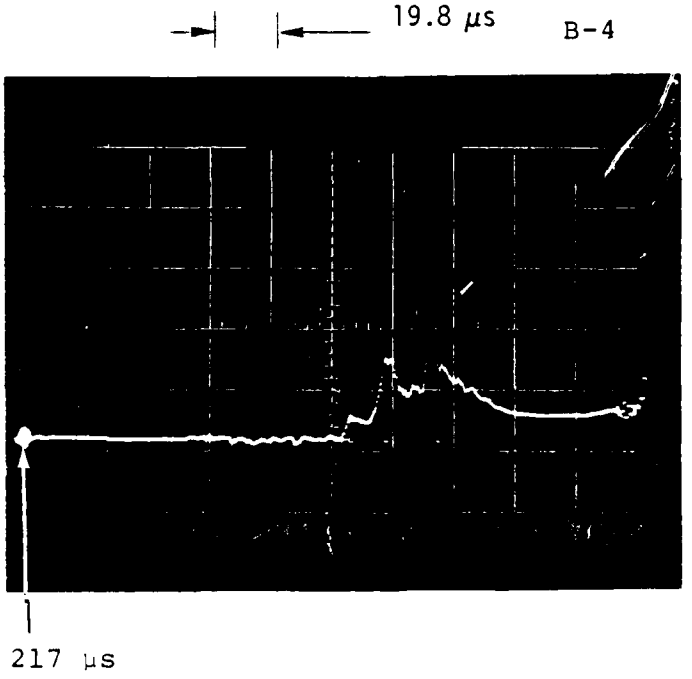

Sweep 19.8 μs/cm

1.05 kbar/cm

(b)

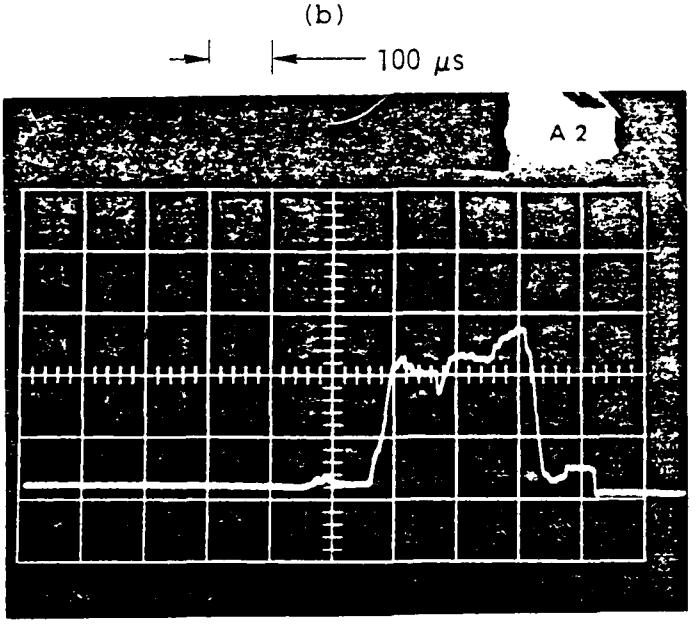

Sweep 100 μs/cm

10.5 kbar/cm

(Bar delay 133 μs)

Figure 22. Gauge Qb-4.

TABLE 3

AIR PRESSURE AT THE TRENCH BOTTOM

Gauge	P_1(kbar)	t_1(μs)	P_2	t_2	P_3	t_3	P_4	t_4
Qb-2	0.35	322	1.15	332	1.32	350	25.3	410
Qb-3	0.34	323	1.12	333	1.68	348	25.0	440
Qb-4	0.42	320	1.42	330	1.73	346	22.3	420

Notes:

1. Collapse began at 248 μs.
2. Initial pipe inside diameter = 26.5 cm.
3. Pressures accurate to ± 10 percent.

(or five) separate pulses visible (seen in Figures 23 and 24) and these are noted in Table 4. The maximum value is markedly less than for those gauges at the pipe bottom. It was anticipated that the lobe air pressure would be less than that on the pipe bottom due to the geometry of the collapse.

Again, a shelf or plateau is in evidence following the third impact in the lobe region. The pressure is ~ 0.1 - 0.5 kbars, again relatively close to the predicted values in this region. This leads further credence to the earlier speculation regarding the collapse. To repeat, this experiment gave some initial low-density blow-off which was sufficient to obscure the light from the argon candle. Underlying this obscuring material it is suggested the collapse is proceeding at a slower velocity more akin to the pre-shot test with its clear boundary between air and pipe wall.

4.5 IMPACT PRESSURE VERSUS TIME AT THE BOTTOM OF THE TRENCH

Two manganin gauges were employed at the bottom of the pipe and the traces are displayed in Figure 25. Gauge M-1 (Figure 25(a)) yields a possible signal with arrival at ~ 410 μs, which is consistent with the beginnings of the main shock arrivals of the bar gauges, as indicated in Figures 20 - 22. The gauge fails at ~ 420 μs. The peak stress at failure is about 12 kbar. Gauge M-2 in Figure 25(b) also apparently started to record a pressure rise at about 400 μs and failed at 410 μs.

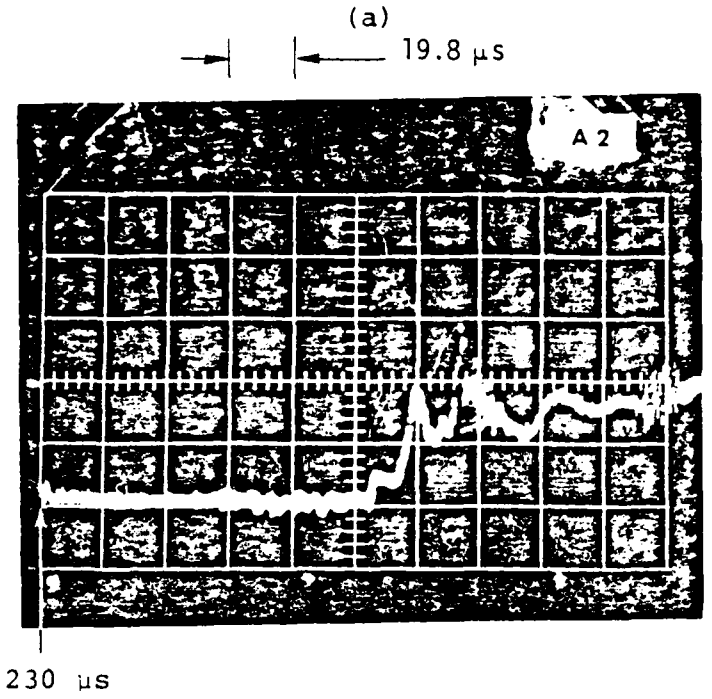

Sweep 19.8 μs/cm

0.103 kbar/cm

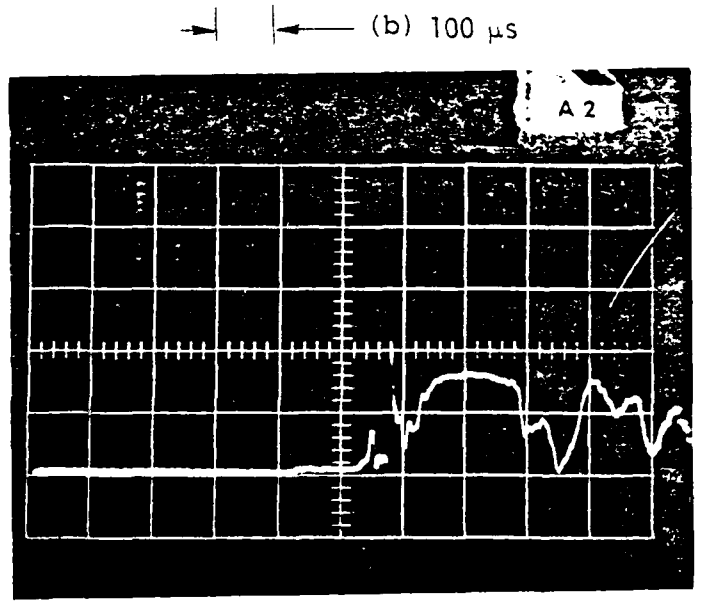

Sweep 100 μs/cm

(+44 μs)

3.09 kbar/cm

(Bar delay 120 μs)

Figure 23. Gauge Qb-1.

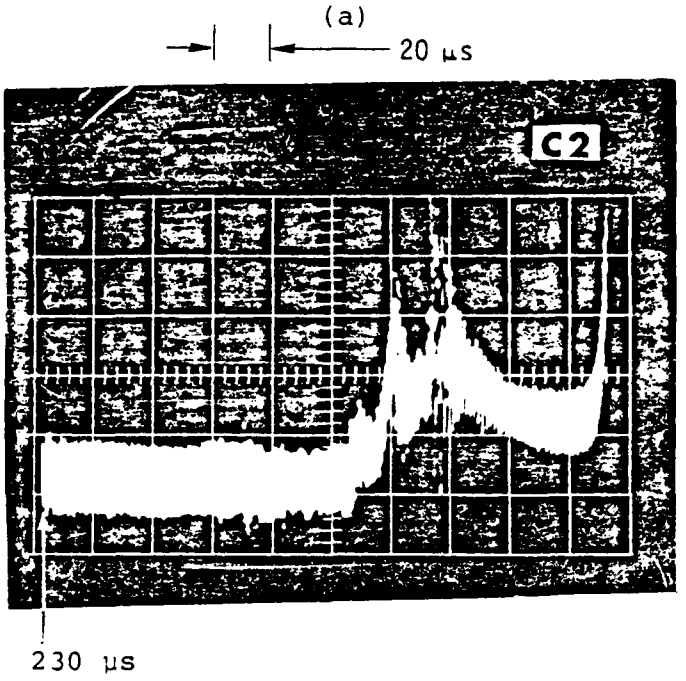

Sweep 20.0 µs/cm

0.111 kbar/cm

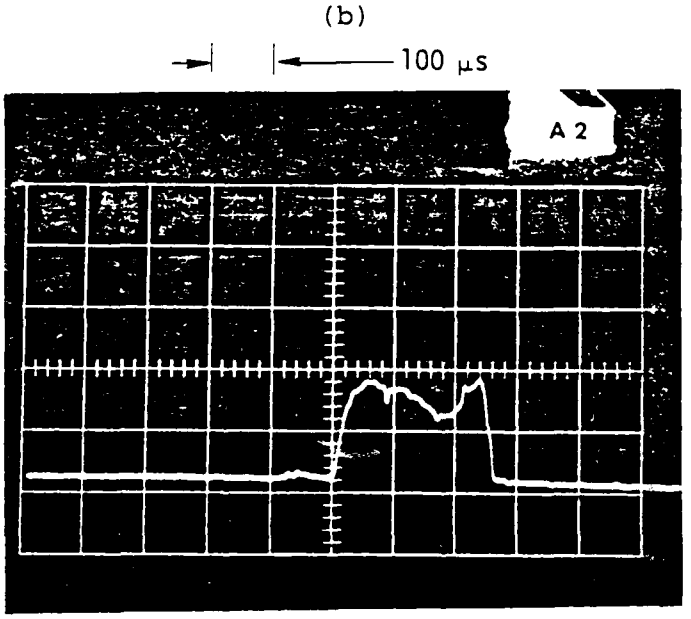

Sweep 100 µs/cm

(+44 µs)

3.33 kbar/cm

(Bar delay 120 µsec)

Figure 24. Gauge Qb-5.

TABLE 4

AIR PRESSURE IN LOBE REGION OF COLLAPSE

Gauge	P_1(kbar)	t_1(μs)	P_2	t_2	P_3	t_3	P_4	t_4
Qb-1	0.054	334	0.185	345	0.288	361	(5.87)	(469)
Qb-2	(0.089)	336	(0.289)	346	(0.400)	364	5.33	439

Note: Pressures accurate to ~ ± 10 percent. Figures in parenthesis are more uncertain due to noise in signal (Qb-5) or anomalous trace (Qb-1) -- see Figures 23 and 24.

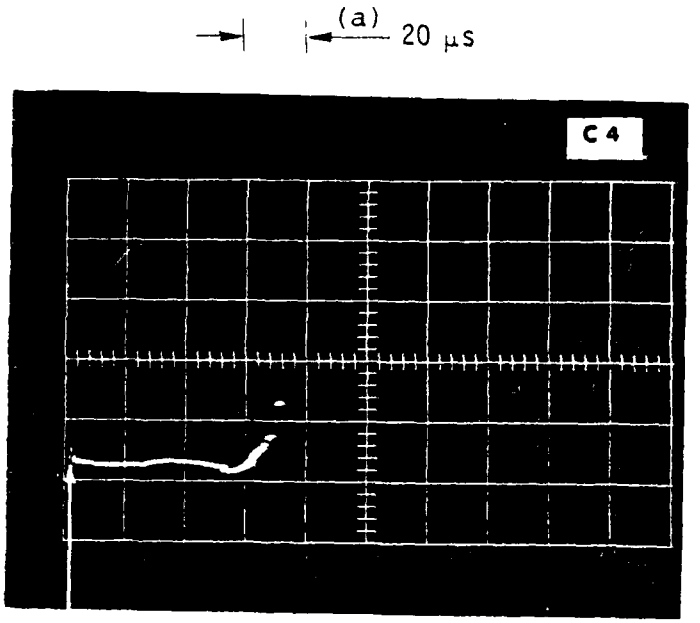

M-1
2 volt/cm
Sweep 20 μs/cm
Main arrived at 410 μs
Fail at 420 μs

350 μs

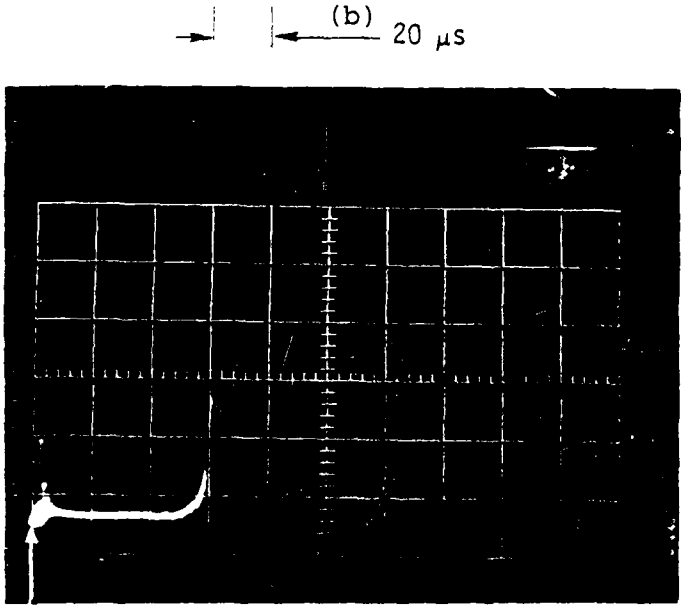

M-2
2 volt/cm
Sweep 20 μs/cm
Main arrived at 400 μs
Fail at 410 μs

350 μs

Figure 25. Manganin gauges M-1 and M-2.

4.6 FREE-FIELD PRESSURE VERSUS TIME AND DEPTH IN THE SOIL UNDER THE HE CHARGE

Five manganin gauges were placed at 10-cm intervals from the surface down to a depth of 40 cm under the HE charge away from the pipe. The goal was to document the pressure pulse which traveled through the soil to enable a determination of the incident pressureat the top of the pipe to be made. The experimental traces are shown in Figures 26 through 29 and readings are listed in Table 5. There are several anomalies in these results which are not understood, but will be described.

Figures 26(a) shows a 3 μs spike followed by a lower amplitude 3 μs oscillation for gauge M-3. The amplitude of the first spike corresponds to a pressure of 135 kbar, beginning at 242 μs. The gauge appears to fail 9 μs later. The spike may represent mainly the shock reverberation in the steel flat pack, if so, a meaningful pressure in the sand was not recorded. A small signal is also seen at 229 μs, but we do not know if it has any significance.

Figure 26(b) shows the record for gauge M-4, which was 10 cm below M3 and slightly below the top of the pipe. A spike of 55 kbar, probably corresponding to the reverberation in steel, is recorded, followed by a peak of 27 kbar and a decay toward the baseline. The negative portion of the trace indicates partial shorting or loss of insulation integrity. The remainder of the record has no pressure significance. The design goal was to hit this depth with a pressure of ~ 65 kbar and our pressure data suggest that we may have reached less than half this value.

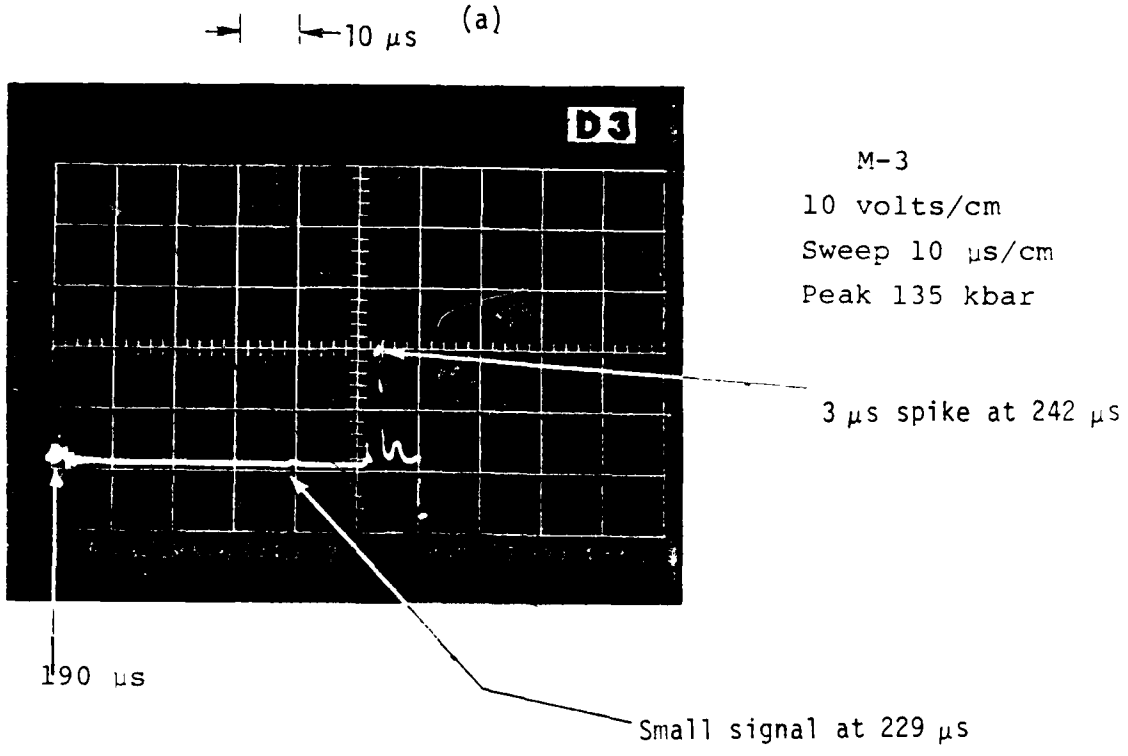

Figure 26. Manganin gauges M-3 and M-4.

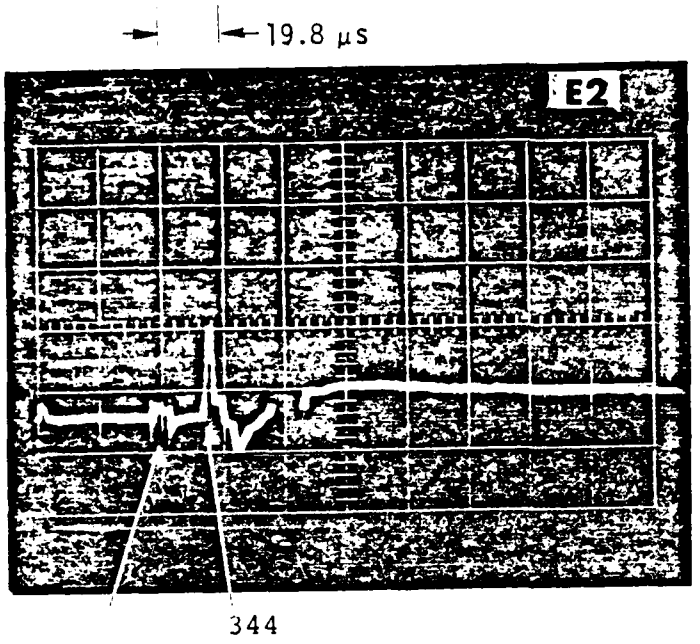

M-5
Sweep 19.8 μs/cm
2.0 volt/cm
Delay = 290 μs

Figure 27. Manganin gauge M-5.

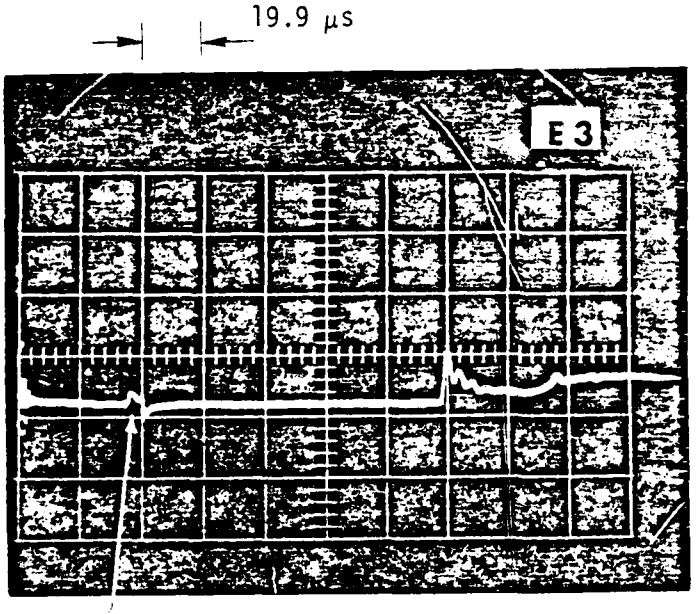

M-6
Sweep 19.9 μs/cm
2.0 volt/cm
Delay = 290 μs

Figure 28. Manganin gauge M-6.

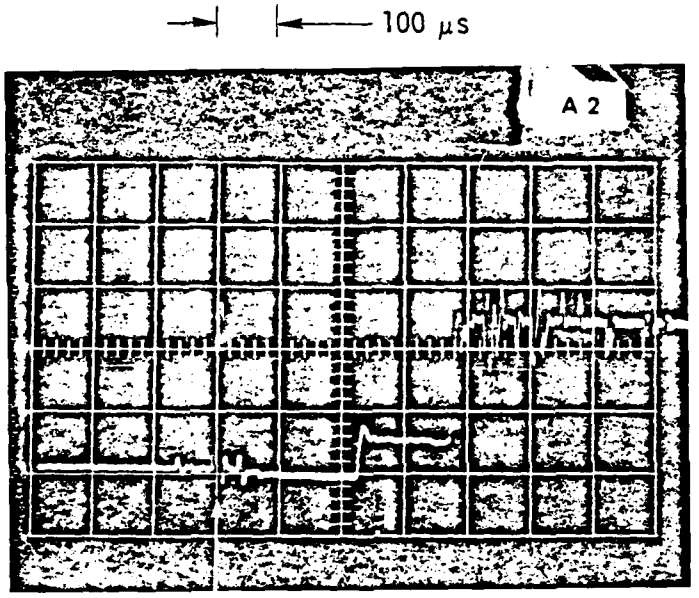

Figure 29. Manganin gauge M-7.

TABLE 5

MANGANIN GAUGE DATA FREE FIELD

Gauge	Depth (cm)	Arrival Time (μs)	Shock Velocity* (mm/μs)	Pressure (kbar)
M-3	0	242	2.2	(135)
M-4	10	288	1.8	(55)
M-5	20	344	1.2	(19)
M-6	30	426	1.1	9.8
M-7	40	520		4.2

* Average between adjacent gauges.

( ) Amplitude of spike influenced by steel gauge package.

Figure 27 shows the sharp pressure spike recorded by gauge M-5. The pressure arrival is at 344 μs. The waveforms appear too short to be valid, except possibly for the 19 kbar peak. The earlier feature at 326 μs is electrical in nature and is seen at the same time in the record for gauge M-6 (Figure 28). The waveform for M-6 looks normal except for the oscillations in the decay. These have a period of 4 μs and probably reflect the steel packaging.

Figure 29 shows the pressure data for gauge M-7. The peak is probably valid, but the constant level after the peak suggests gauge element stretching.

A major inconsistency in the manganin gauge data is timing. Gauge M-3 is hit only 6 μs before the camera shows the pipe collapse began. Gauge M-4 shows pressure arrival 40 μs after the pipe starts to move, whereas these two events should occur at nearly the same time. We have not resolved this time discrepancy.

The relative times between arrivals at the various manganin gauges, however, yield shock velocities that vary smoothly between 2.2 mm/μs for the first two gauges to 1.1 mm/μs for the last two. Figure 30 shows time of arrival versus depth. Noted on Figure 30 is the shock arrival at the inside-top of the pipe (9.6 cm from the surface) as shown by the optical data. The first manganin gauge at the surface is only reporting a signal at about the time the main shock is 9.6 cm deep. A timing error of some sort is suggested, but we have been unable to locate it.

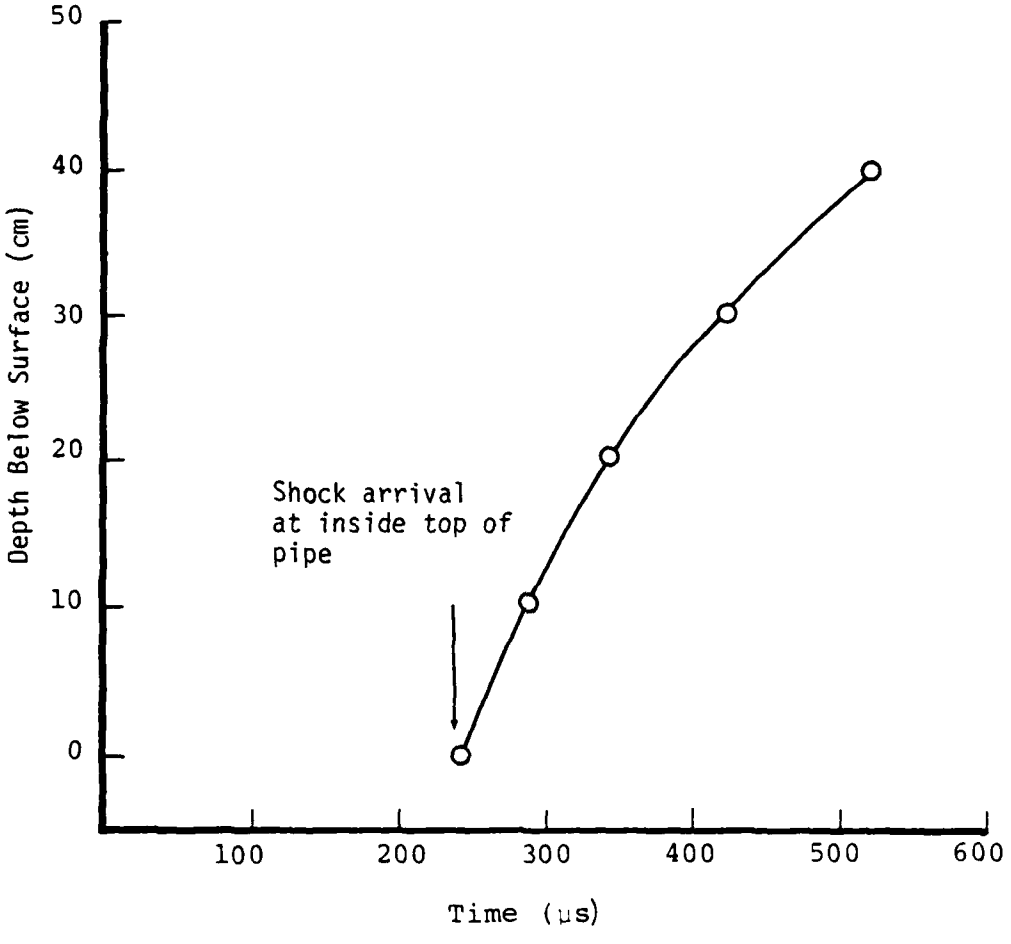

Figure 30. Time of arrival versus depth for manganin gauges.

4.7 AIR PRESSURE VERSUS TIME IN PIPE OUTSIDE RAPID CLOSURE REGION

Four low pressure quartz gauges were placed at 150, 250, 350 and 450 cm down-pipe from the center of the charge. (There were also TOA gauges at these points.) An additional two pressure gauges were placed 150 and 250 cm up-pipe from the charge (toward the argon candle). Data return from these gauges was poor. Figure 31 shows the trace for gauge Qp-1 at a distance of 150 cm from the center of collapse. What is interpreted as shock arrival is indicated on the trace. The pressure level appears to be about 34 bars, as measured from the negative excursion. This interpretation is considered doubtful because the pressure inferred from the TOA gauges is about 10 bars. This will be examined further in the section detailing the TOA data.

Figure 32 shows the trace for gauge Qp-2 at a distance of 250 cm. Again, what we interpret as shock arrival is indicated. (On both these gauges it is not clear we could have picked out the signal without knowing the TOA from the pin gauges.)

Figure 33 shows gauge Qp-3 (350 cm) which has no useful signals. Qp-3 appears to be responding between 4 and 5 ms, but the interpretation is debatable. No record was obtained from Qp-4 (450 cm).

Figure 34 details gauges Qp-5 (150 cm up-pipe) and Qp-6 (250 cm up-pipe). Figure 34(b) is the only quartz gauge showing what might be a clear unambiguous pressure signal. The time of arrival and signal level are indicated on this figure. As will be shown in a later section, this pressure is generally consistent with shock velocity information.

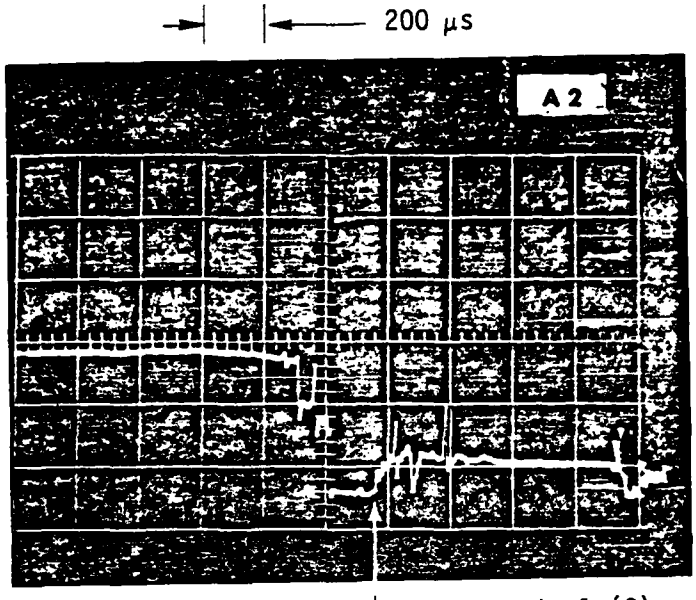

Sweep: 200 μs/cm
56 bar/cm

Figure 31. Quartz pressure gauge Qp-1.

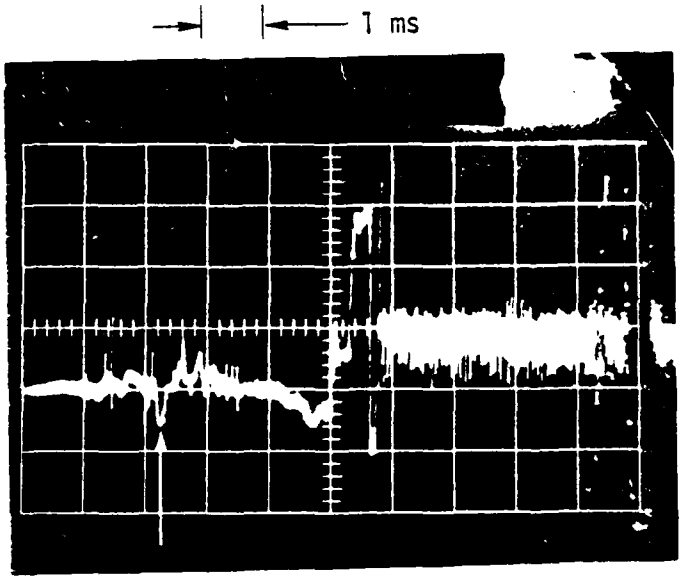

Sweep: 1 ms/cm
18 bar/cm

Figure 32. Quartz pressure gauge Qp-2.

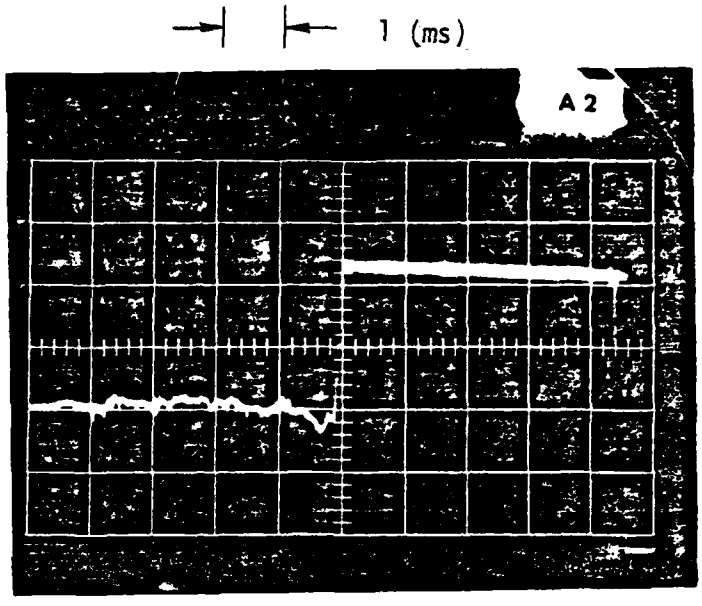

Qp-3
Sweep 1 ms/cm
.022 kbar/cm

No useful signal

Figure 33. Quartz pressure gauge Qp-3.

(a) Qp-5

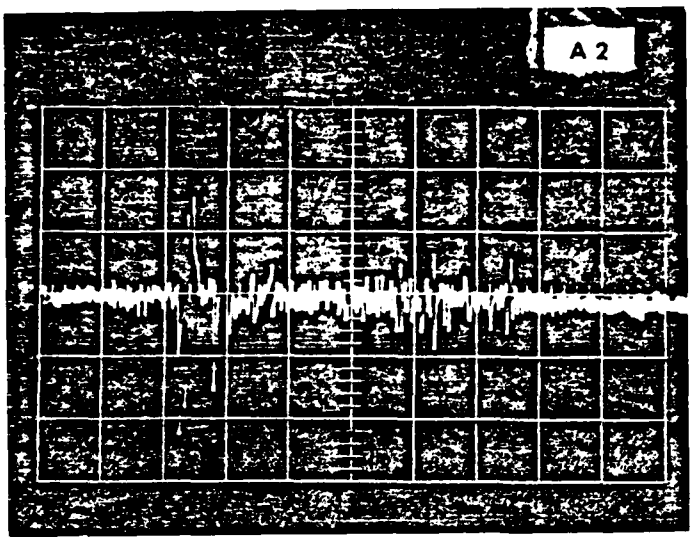

Sweep: 200 μs/cm

.056 kbar/cm

No detectable signal

(b) Qp-6

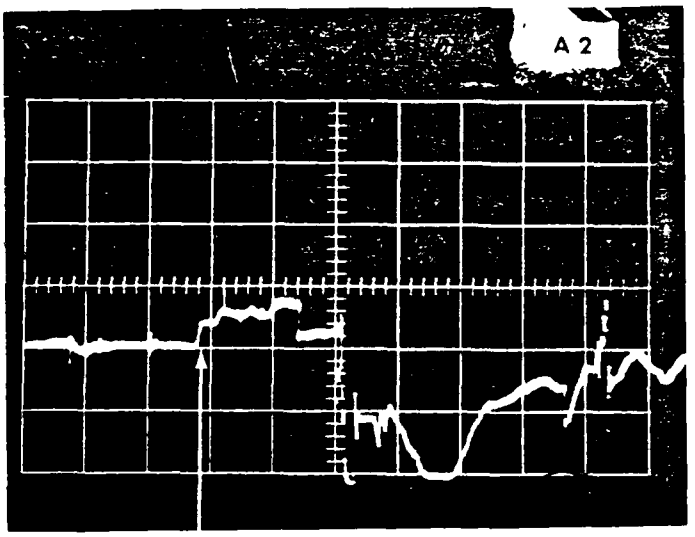

Sweep: 1 ms/cm

.021 kbar/cm

Shock arrival
2.67 ms

Figure 34. Quartz pressure gauges Qp-5 and Qp-6.

4.8 TIME OF ARRIVAL OF PRESSURE WAVE IN PIPE OUTSIDE RAPID CLOSURE REGION

Three of the four PZT pin probes gave useful data which, combined with the time of closure of the pipe, seem consistent. Table 6 lists the TOA results with comments. The gauge traces are shown in Figures 35 and 36.

Figure 37(a) is a plot of the TOA data. The quartz gauge data is also shown showing its seeming consistency. The point at 60 cm represents the main shock arrival at the bar gauges. The shock velocity is seen to be asymptotic to the sound velocity as required. Figure 37(b) is a schematic of the pipe showing the collapsed region.

Even though only marginal pressure data was obtained, this TOA information allows the pressure to be inferred from the measured shock velocities. Using an appropriate equation-of-state for air (see Figure 38), shock pressures are obtained directly from the shock velocities. These results are presented in Figure 39 as the large dots (triangles are the possible data from the pressure gauges). For reference a curve with P_{α} 1/R (normalized to the pressure at 200 cm since the TOA gauges surrounding this point gave sharp results) has been drawn in.

The air-shock pressures are quite low. At 10 pipe diameters (noted in the figure) from the center of the HE the overpressure is ~ 483 KPa (70 psi). By the time the shock reaches the last TOA gauge, the shock is moving sonically at overpressures $\leq$ 69 KPa (10 psi). This TOA data would seem to imply that rapid ceiling collapse is not an effective means of coupling energy down the

TABLE 6

TIME OF ARRIVAL VERSUS RANGE

Location	Range	TOA
Edge of rapid collapse (from bar gauges)	60 cm	0.44 ms
Probe 1	150 cm	1.33 ms[1]
Probe 2	250 cm	2.51 ms[1]
Probe 3	350 cm	Unresolvable noise
Probe 4	450 cm	6.5 ms[2]

Notes: 1. Clean, sharp signal - no ambiguity

2 Great deal of noise on this probe, but there is a rise at the time indicated which may be consistent with the other times measured.

(a) TOA-1

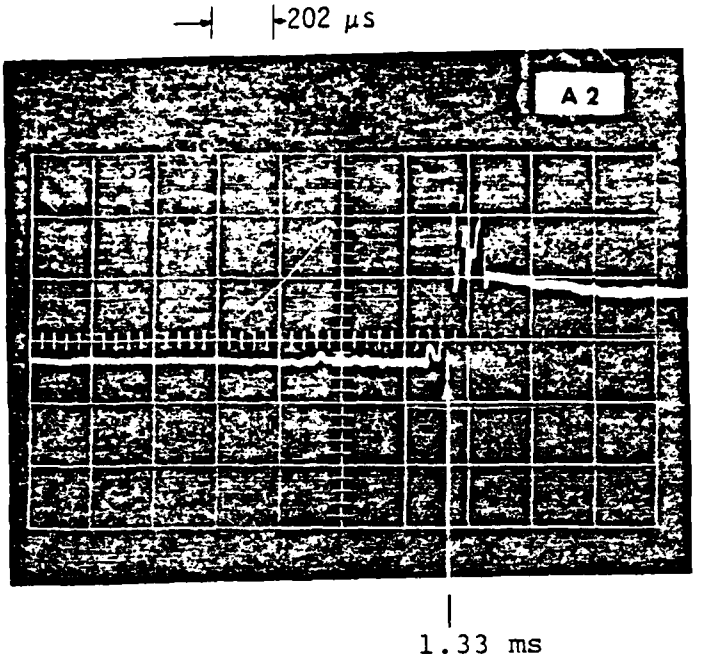

(b) TOA-2

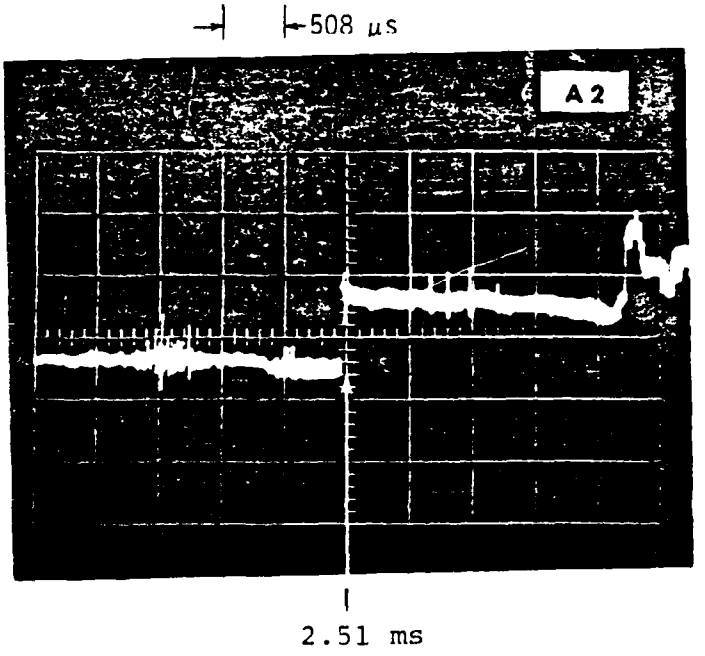

Figure 35. TOA gauges 1 and 2.

(a) TOA-3

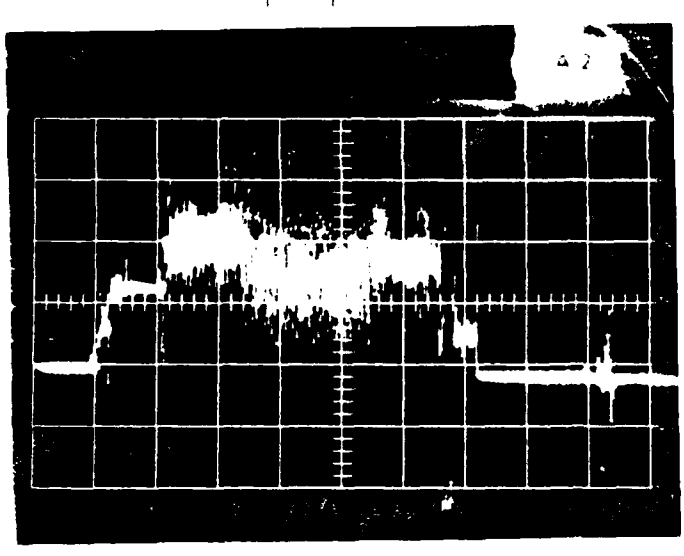

Sweep: 1.01 ms/cm

No detectable signal

(b) TOA-4

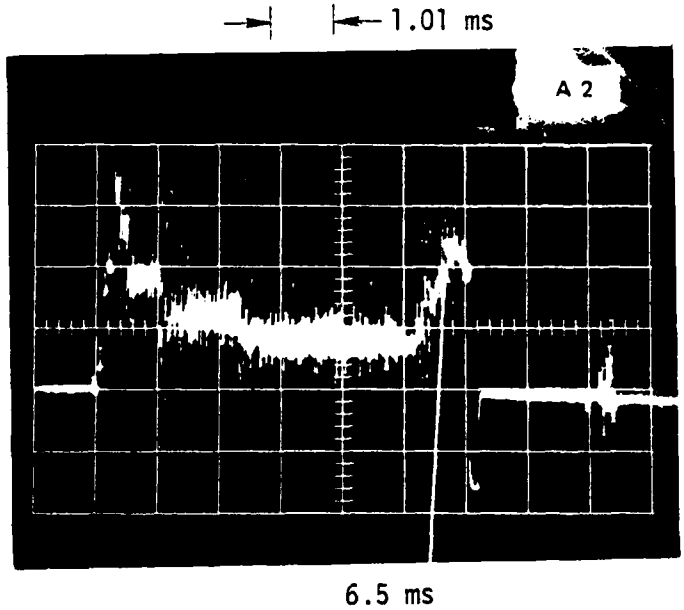

Sweep: 1.01 ms/cm

6.5 ms

Figure 36. TOA gauges 3 and 4.

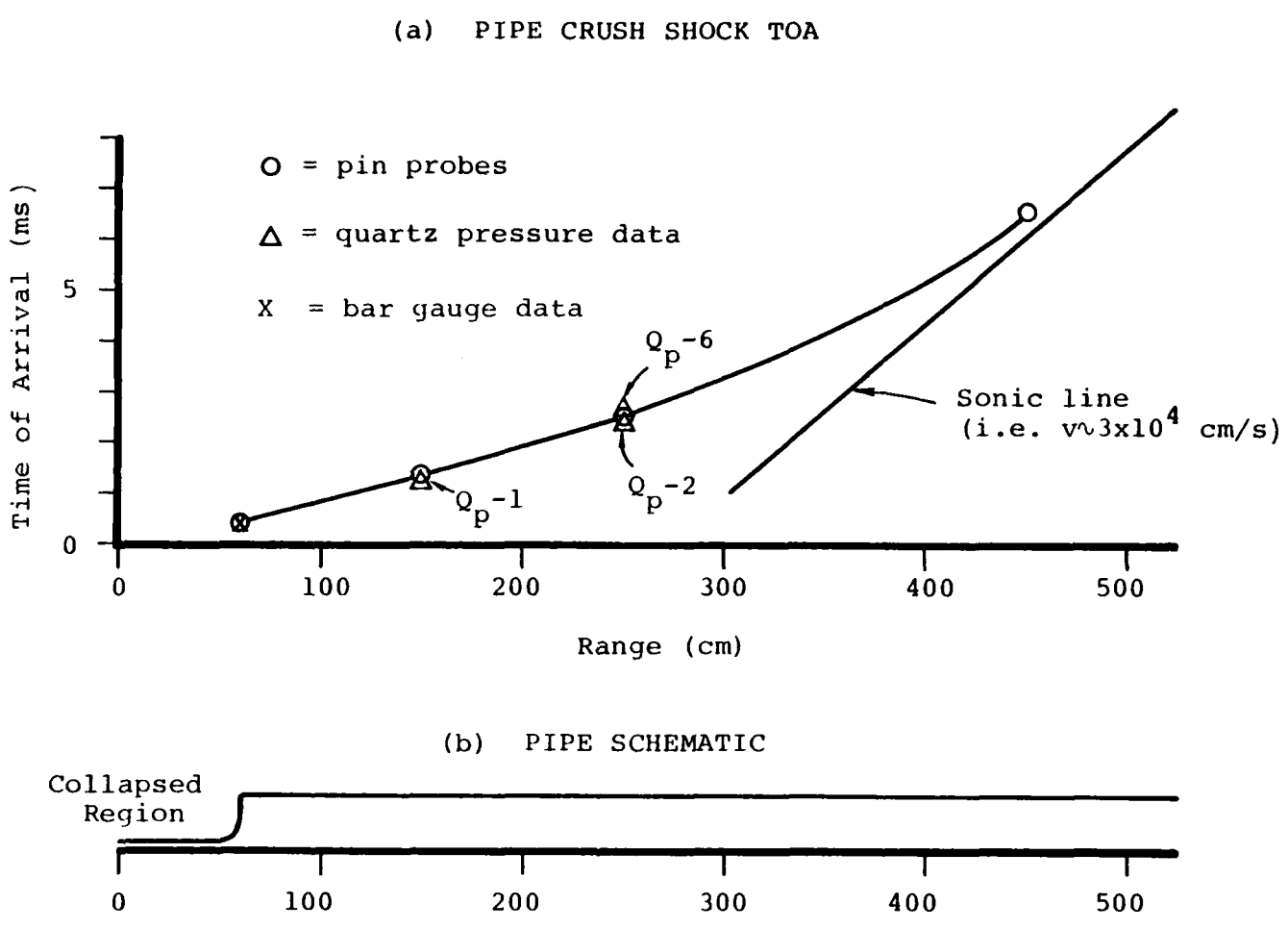

Figure 37. Time of arrival (TOA) for air shock down pipe.

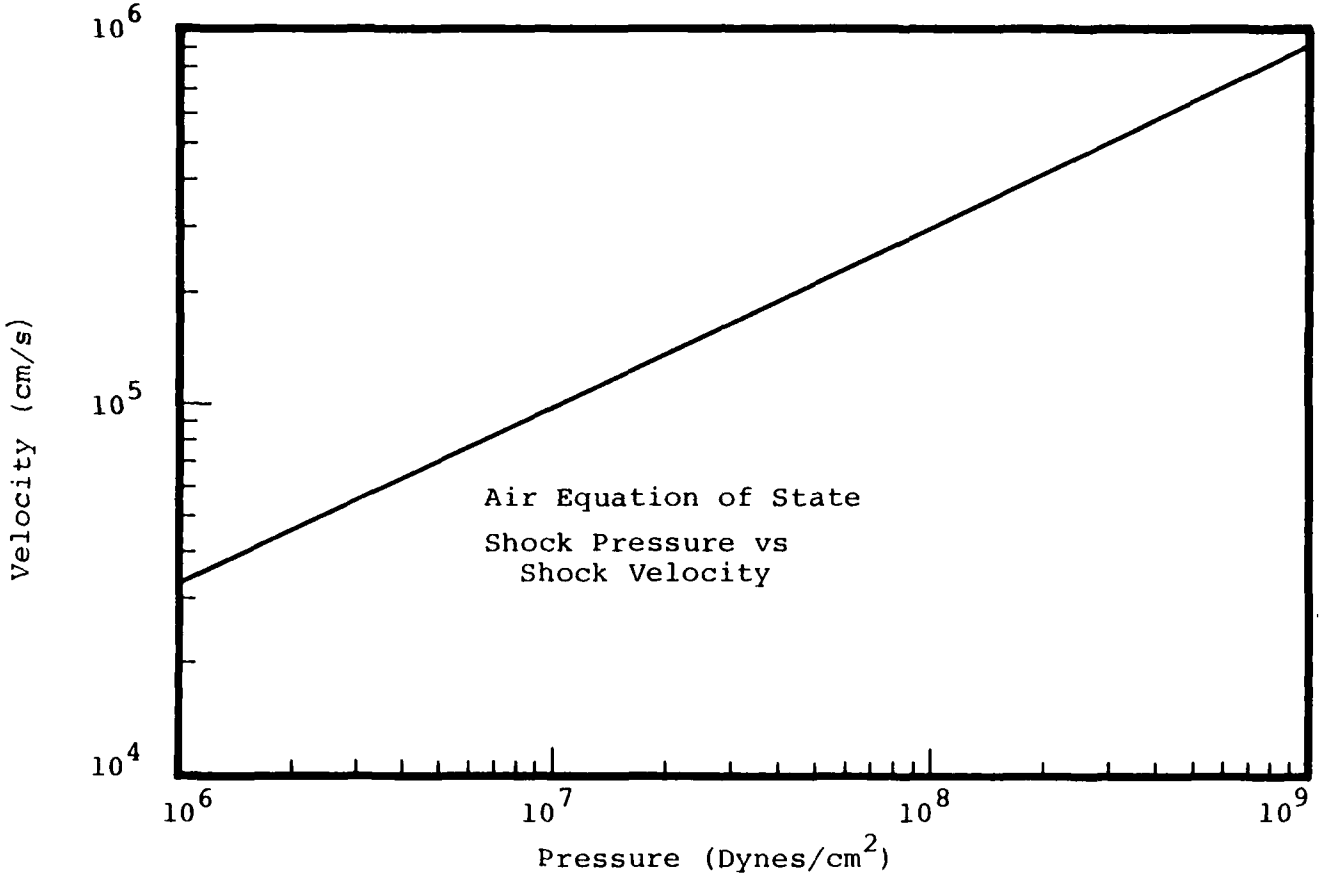

Figure 38 . Shock pressure as a function of shock velocity for air.

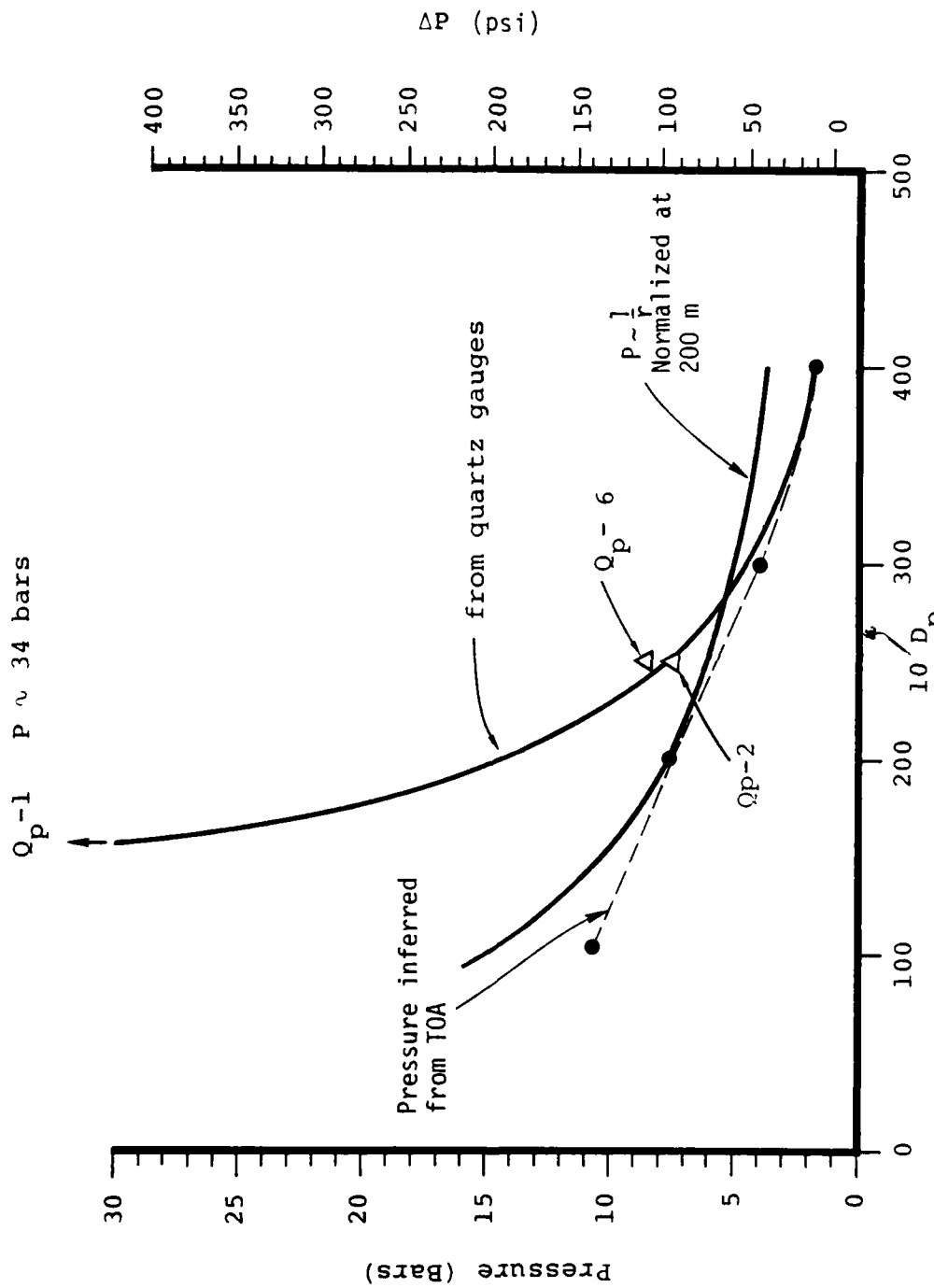

Figure 39 . Pipe crush pressures based on TOA.

pipe. Even if one only accepts TOA from gauges 1 and 2, and then takes a 1/R fall-off, the overpressure at pipe's end (15 D pipe) is ~ 276 KPa (40 psi).

The quartz pressure gauge data is also shown in this figure. The first point at 150 cm is significantly higher than that obtained from shock velocity information. The points at 250 cm are more consistent with the TOA-inferred pressures. Based on the otherwise consistent information, it appears that the first pressure gauge, with its unusual trace, probably is not valid. The undershoot preceding the main pulse visible on the second gauge is undoubtedly present on the first gauge, resulting in a false baseline and thus a higher reading for the pressure. All the quartz-pressure data seem marginal at best (except, perhaps for gauge Qp-6) and the fact that air is easily characterized with an equation-of-state yielding shock pressure as a function of shock velocity gives more weight to the TOA-inferred pressures.

SECTION 5.

SUMMARY AND CONCLUSIONS

In an attempt to address the question of energy coupled into an MX-trench from a strong ground-shock induced trench collapse, S^3 designed and executed a 1/16-scale trench experiment where the collapse was driven by a suitably chosen HE charge. Design calculations indicated the configuration necessary to simulate the effect of a 1 megaton surface burst 12.5 meters from an MX-trench. The nuclear conditions were obtained from an extensive, two-dimensional, radiation-hydrodynamics calculation performed by S^3 called Source 3/5. A further two-dimensional calculation was done on the experimental configuration to attempt to define and predict the mode and strength of collapse.

Two pre-shot experiments were initated to assure good performance of the main diagnostic on the experiment; namely, optical, framing-camera photos to observe the collapse mode. The main experiment test-bed contained numerous other diagnostics as well, including bar gauges to measure pressure at the bottom of the pipe under the HE charge and TOA gauges along the uncollapsed section of pipe to define the shock driven into the pipe air by the rapid collapse, which was the main motivation for the experiment.

The two-dimensional calculation suggested tha the collapse would leave lobes of air off-axis, implying that the effectiveness in driving a shock down the pipe might be low. The pre-shot tests seemed to confirm this mode of collapse, but since they had no down-pipe diagnostics, the question of effectiveness remained open.

The main experiment gave some initial surprises regarding collapse mode, but a cross-correlation of the various diagnostics that yielded believable results seemed to confirm the implications of the calculations. The framing camera photos appeared to indicate more rapid collapse than expected, but on examining the bar gauge data, the optically obscuring material was very low-density dust. The main mass of the pipe wall seemed to be moving at about the predicted velocity (and that observed in the pre-shot tests). The appearance of this dust may have been due to either a thinner pipe wall in the main experiment or to the presence of filled joints in the pipe sections under the HE charge. The bar gauge data was in good agreement with that expected from the calculation. Manganin gauges at the bottom of the pipe and in the soil beside the pipe below the HE gave ambiguous results.

The low-pressure quartz gauges gave generally little or no information, but what there was may be consistent with that inferred from the TOA gauges. The data from these time-of-arrival measurements appear reliable. Determining a shock pressure from the shock velocity gives a consistent set of pressure values down the pipe and the potentially acceptable direct pressure measurements are generally in agreement with these values. At a distance of 10 pipe diameters, the trench air shock is ~ 483 KPa (70 psi) overpressure, quite low relative to the design parameters for the trench.

The results of the manganin gauges in the free-field pressure measurements should not be allowed to obscure conclusions which may be drawn from this experiment. Even if the trench was impacted with the lower shock pressure of ~ 3.5 GPa (35 kbars) rather than the design goal of 9 GPa (90 kbars), the mode of collapse seems to be verified. That is, lobes of air are left at the sides of the

collapse, so the mass of air directly under the rapid collapse region is not compressed uniformly at the same time. This collapse geometry is not conducive to driving as strong a shock down-pipe as a more nearly planar roof collapse would. It should be emphasized that the manganin gauge data have anomalies which call into doubt the reliability of any of their results. (In addition, the inferred velocity of trench collapse appears to agree with predictions based on a 9 GPa impact.)

To answer the motivating question, it appears that strong ground shock-induced trench collapse is <u>not</u> an efficient method for coupling energy down the trench and does not pose a stressing design environment.

SECTION 6.

REFERENCES

1. "A Review of MX Trench Testing Requirements," A Report of the Findings of the Joint DNA, SAMSO and AFWL 30 Day Group, November 1977.

2. Coleman, P. L. and H. R. Kratz, "HYBLA GOLD Measurements: Plasma, Ablation and Pipe Expansion," Systems, Science and Software Report SSS-R-79-3850, 1978.

DISTRIBUTION LIST

DEPARTMENT OF DEFENSE

Assistant to the Secretary of Defense
Atomic Energy
ATTN: Executive Assistant

Defense Advanced Rsch Proj Agency
ATTN: TIO

Defense Intelligence Agency
ATTN: RDS-3A

Defense Nuclear Agency
ATTN: SPSS
ATTN: DDST
2 cy ATTN: SPSS, G. Ullrich
4 cy ATTN: TITL

Defense Technical Information Center
12 cy ATTN: DD

Field Command
Defense Nuclear Agency
ATTN: FCTMD
ATTN: FCPR

Field Command
Defense Nuclear Agency
Livermore Division
ATTN: FCPRL

Joint Strat Tgt Planning Staff
ATTN: NRI-STINFO Library
ATTN: XPFS

Undersecretary of Def for Rsch & Engrg
ATTN: Strategic & Space Systems (OS)

DEPARTMENT OF THE ARMY

BMD Advanced Technology Center
Department of the Army
ATTN: ATC-T

BMD Systems Command
Department of the Army
ATTN: BMDSC-HW

Chief of Engineers
Department of the Army
ATTN: DAEN-ASI-L
ATTN: DAEN-RDM
ATTN: DAEN-MPE-T, D. Reynolds
ATTN: DAEN-RDL

Harry Diamond Laboratories
Department of the Army
ATTN: DELHD-I-TL
ATTN: DELHD-N-P

U.S. Army Ballistic Research Labs
ATTN: DRDAR-TSB-S
ATTN: DRDAR-BLE, J. Keefer

U.S. Army Cold Region Res Engr Lab
ATTN: Library

DEPARTMENT OF THE ARMY (Continued)

U.S. Army Construction Engrg Res Lab
ATTN: Library

U.S. Army Engineer Center
ATTN: Technical Library

U.S. Army Engr Waterways Exper Station
ATTN: WESSA, W. Flathau
ATTN: WESSD, G. Jackson
ATTN: J. Zelasko
ATTN: Library

U.S. Army Material & Mechanics Rsch Ctr
ATTN: Technical Library

U.S. Army Materiel Dev & Readiness Cmd
ATTN: DRXAM-TL

U.S. Army Nuclear & Chemical Agency
ATTN: J. Simms
ATTN: Library

DEPARTMENT OF THE NAVY

Naval Construction Battalion Center
ATTN: Code L51, J. Crawford
ATTN: Code L08A
ATTN: Code L53, J. Forrest

Naval Facilities Engineering Command
ATTN: Code 09M22C

Naval Postgraduate School
ATTN: Code 0142 Library
ATTN: G. Lindsay

Naval Research Laboratory
ATTN: Code 2627

Naval Surface Weapons Center
White Oak Laboratory
ATTN: Code F31
ATTN: Code X211

Naval Surface Weapons Center
ATTN: Tech Library & Info Svcs Br

Office of Naval Research
ATTN: Code 715

DEPARTMENT OF THE AIR FORCE

Air Force Institute of Technology
Air University
ATTN: Library

Air Force Systems Command
ATTN: DLWM

Assistant Chief of Staff
Intelligence
Department of the Air Force
ATTN: IN

DEPARTMENT OF THE AIR FORCE (Continued)

Air Force Weapons Laboratory
Air Force Systems Command
ATTN: NTE, M. Plamondon
ATTN: SUL
ATTN: NTV, D. Payton
ATTN: NTED-I
ATTN: NTED-A
ATTN: DEY
ATTN: NTES-S
ATTN: NTES-G
ATTN: NTEO

Assistant Secretary of the Air Force
Research, Development & Logistics
Department of the Air Force
ATTN: SAFALR/DEP for Strat & Space Sys

Ballistic Missile Office
Air Force Systems Command
ATTN: MNNXH, D. Gage
ATTN: MNNX, W. Crabtree
ATTN: MNNXH, M. Delvecchio

Deputy Chief of Staff
Research, Development, & Acq
Department of the Air Force
ATTN: AFRDQA
ATTN: AFRDPN
ATTN: AFRDQI
ATTN: AFRDQI, N. Alexandrow

Strategic Air Command/XPFS
Department of the Air Force
ATTN: NRI-STINFO Library
ATTN: XPFS

VELA Seismology Center
Department of the Air Force
ATTN: G. Ullrich

DEPARTMENT OF ENERGY CONTRACTORS

Lawrence Livermore National Laboratory
ATTN: D. Glenn

Los Alamos National Scientific Laboratory
ATTN: C. Keller
ATTN: R. Sanford

Sandia National Laboratories
ATTN: A. Chabai
ATTN: Org 1250, W. Brown

DEPARTMENT OF DEFENSE CONTRACTORS

Acurex Corp
ATTN: J. Stockton
ATTN: K. Triebes
ATTN: C. Wolf

Aerospace Corp
ATTN: H. Mirels
ATTN: Technical Information Services

Agbabian Associates
ATTN: M. Agbabian

Applied Theory, Inc
2 cy ATTN: J. Trulio

DEPARTMENT OF DEFENSE CONTRACTORS (Continued)

Artec Associates, Inc
ATTN: S. Gill

Boeing Co
ATTN: Aerospace Library
ATTN: S. Strack

California Research & Technology, Inc
ATTN: M. Rosenblatt
ATTN: Library

Civil Systems Inc
ATTN: S. Melzer

University of Denver
Space Science Lab
ATTN: J. Wisotski

Eric H. Wang
Civil Engineering Rsch Fac
University of New Mexico
ATTN: P. Lodde
ATTN: J. Lamb
ATTN: J. Kovarna

General Electric Company—TEMPO
ATTN: DASIAC

H-Tech Labs, Inc
ATTN: B. Hartenbaum

Higgins, Auld & Associates
ATTN: N. Higgins
ATTN: H. Auld
ATTN: J. Bratton

IIT Research Institute
ATTN: Documents Library

J. H. Wiggins Co, Inc
ATTN: J. Collins

Kaman AviDyne
ATTN: R. Ruetenik

Merritt CASES, Inc
ATTN: Library

Mission Research Corp
ATTN: G. McCartor
ATTN: C. Longmire

Nathan M. Newmark Consult Eng Svcs
ATTN: N. Newmark
ATTN: W. Hall

Pacific-Sierra Research Corp
ATTN: H. Brode

Pacifica Technology
ATTN: R. Allen
ATTN: Library

Physics International Co
ATTN: F. Sauer
ATTN: Technical Library
ATTN: J. Thomsen

DEPARTMENT OF DEFENSE CONTRACTORS (Continued)

R & D Associates
ATTN: Technical Information Center
ATTN: J. Carpenter
ATTN: J. Lewis
ATTN: C. MacDonald
ATTN: A. Kuhl
ATTN: R. Port
ATTN: P. Haas

Science Applications, Inc
ATTN: H. Wilson
ATTN: Technical Library
ATTN: R. Schlaug

Science Applications, Inc
ATTN: D. Hove

Science Applications, Inc
ATTN: B. Chambers III

SRI International
ATTN: G. Abrahamson
ATTN: D. Johnson
ATTN: J. Colton
ATTN: Library

Systems, Science & Software, Inc
ATTN: C. Needham

DEPARTMENT OF DEFENSE CONTRACTORS (Continued)

Systems, Science & Software, Inc
ATTN: K. Pyatt
ATTN: J. Barthel
ATTN: Library

Systems, Science & Software, Inc
ATTN: J. Murphy

Systems, Science & Software, Inc
ATTN: C. Hastings

Terra Tek, Inc
ATTN: Library
ATTN: A. Abou-Sayed

TRW Defense & Space Sys Group
ATTN: Technical Information Center
ATTN: T. Mazzola
ATTN: N. Lipner

TRW Defense & Space Sys Group
ATTN: G. Hulcher

Weidlinger Assoc, Consulting Engineers
ATTN: I. Sandler

Weidlinger Assoc, Consulting Engineers
ATTN: J. Isenberg

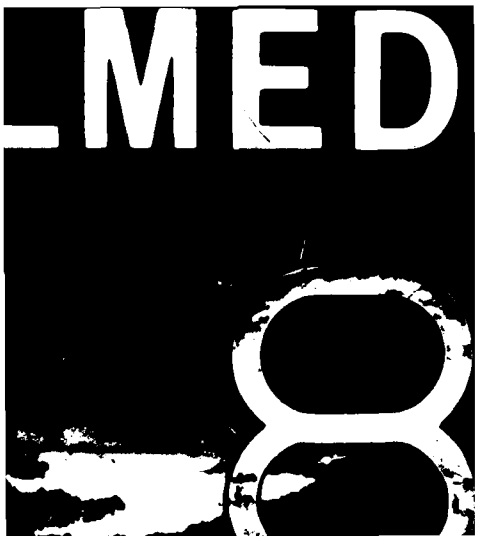
LMED